Precambrian Research 410 (2024) 107469

Contents lists available at ScienceDirect

Precambrian Research

journal homepage: www.elsevier.com/locate/precamres

50th Anniversary Invited Review

Passive continental margin subducted to mantle depths: Coesite-bearing metasedimentary rocks from the Neoproterozoic Brasília Orogen, West Gondwana margin

Mario da Costa Campos Neto [a,*], Gabriella Labate Frugis [a], Alice Westin [a], Renaud Caby [b], Augusto G. Nobre [c], Olivier Brugier [b], Rômulo A. Ando [d]

[a] Instituto de Geociências, Universidade de São Paulo, 05508-080 São Paulo, Brazil
[b] Géosciences Montpellier, Université de Montpellier, CNRS-UMR 5243, Place Eugéne Bataillon, 34095 Montepellier Cedex 5, France
[c] Departamento de Geociências, Centro de Ciências Naturais e Exatas, Universidade Federal de Santa Maria, Avenida Roraima, 1000, 97105900 Santa Maria, RS, Brazil
[d] Laboratório de Espectroscopia Molecular, Departamento de Química Fundamental, Instituto de Química, Universidade de São Paulo, Avenida Prof. Lineu Prestes, 748, 05508-000 São Paulo, SP, Brazil

ARTICLE INFO

Keywords:
UHPM
Microcoesite inclusions on garnet
Rt-Ky-Grt-KFels granulite
Zr-Mnz-Rt U-Pb dating
Cryogenian-Ediacaran collision
Prolonged metamorphic evolution

ABSTRACT

In this contribution, we investigate the ultra-high pressure metamorphism (UHPM), and subsequent pressure–temperature-time (P-T-t) exhumation path recorded by granulites (rutile-kyanite-garnet-Kfeldspar and rutile-titanite-hornblende-garnet gneisses) of a coherent thrust package (Três Pontas-Varginha Nappe) of the southernmost edge of the Brasília Orogen. The Brasília Orogen, along with Northern Borborema Province, Dahomey, and Hoggar Belts, comprise a widespread linear system of orogens developed during the West Gondwana assembly, recording the diachronic closure of the Tonian-Ediacaran long-lived Goiás-Pharusian Ocean. Optical petrography, Raman spectroscopy, mineral chemistry, Ti-in-zircon and Zr-in-rutile thermometry, and U-Pb dating (LA-ICP-MS) of zircon, monazite, and rutile were combined to identify UHP minerals and textures and to track the decompression/exhumation path. Garnet porphyroblasts preserve UHPM chemical domains and are often radially fractured around rounded quartz inclusions. Remnants of microcoesite were detected by Raman spectroscopy within these inclusions, identified by the diagnostic bands at approximately 170 cm^{-1}, 270 cm^{-1}, and 520 cm^{-1}. Coesite remnants were identified across the nappe stack along with 60° angle-oriented rutile needle inclusions in garnet, which suggests exsolution from Ti-bearing UHP garnets. Soccer ball zircon crystals of Ky-bearing granulites, with flat HREE pattern and negative Eu anomaly, yielded a U-Pb age of around 620 Ma. This age is interpreted as the record of the granulite facies metamorphism (750–805 °C and 15 kbar) post-dating the UHPM from the subduction channel. Zircon and monazite record exhumation under high temperatures around 595–590 Ma, and rutile crystals record the final stages of the decompression path from 590 to 585 Ma. Monazite crystallization occurred until 570 Ma. The new data combined with previously reported metamorphic paths, record a time interval of about 25 m.y. for the exhumation of the Tres Pontas-Varginha Nappe under subsolidus conditions. Our findings represent one of the oldest reports of Neoproterozoic coesite-forming UHPM recorded in metasedimentary rocks buried to mantle depths in the subduction of the passive continental margin.

1. Introduction

Evidence of ultrahigh-pressure metamorphism (UHPM) in the geological record has important implications for unraveling Earth's geodynamic evolution, such as the onset of deep subduction. The subduction of continental crust rocks to greater depths up to the mantle transition is recorded by exhumed rocks containing relics of ultrahigh-pressure minerals. The main UHP mineral indicators are the high-pressure polymorphs of silica and carbon, such as coesite and micro-diamond, respectively (Chopin, 2003, 1984; Dobrzhinetskaya and Faryad, 2011).

Phanerozoic UHPM is recorded by mineral textures of decompression, such as exsolution lamellae of spinel, kyanite, and rutile in quartz interpreted as evidence of substitution of former stishovite, or

* Corresponding author.
E-mail address: camposnt@usp.br (M. da Costa Campos Neto).

https://doi.org/10.1016/j.precamres.2024.107469
Received 27 February 2024; Received in revised form 21 May 2024; Accepted 5 June 2024
Available online 12 June 2024

clinopyroxene, rutile, and apatite exsolution in garnet. They were described respectively in the Paleozoic rocks of the Altyn Tagh, western China (Liu et al., 2007), and in the Triassic eclogites of Yangkou, Sulu orogen (Ye et al., 2000; Zheng et al., 2019). Other significant Phanerozoic UHP rock occurrences are the Western Alps (Chopin, 1984; Manzotti et al., 2022), the Kaghan Valley in the Himalayas (O'Brien et al., 2001), the Edough Massif in Algerie (Caby et al., 2014), the Western Gneiss Region of Norway (Kylander-Clark et al., 2012; Smith, 1984), the Kokchetav Massif in Kazakhstan (Parkinson and Katayama, 1999; Sobolev and Shatsky, 1990; Stepanov et al., 2016), the Saxonian Ergebirge in the Bohemian Massif (Massonne, 2003), and the fast exhumed Pliocene Papua New Guinea eclogite (Baldwin et al., 2004; Faryad et al., 2019). These Phanerozoic UHP–HP rocks indicate the occurrence of deep subduction processes since the Cambrian. The mantle source of hydrothermal fluxes in lithosphere-scale shear zones is recorded in the southeastern Tibetan Plateau (Zhang et al., 2022, 2021). Nonetheless, the findings of Neoproterozoic coesite-bearing mafic metamorphic rocks of continental origin (Caby, 1994; Ganade et al., 2023; Gomes et al., 2023; Jahn et al., 2001; Santos et al., 2015, 2009) extends to older ages the convergent geodynamic processes of plate tectonics observed in the Phanerozoic.

The burial and consumption of the continental crust to the depths of the deep mantle, regardless of its lower density, is reproduced by experimental data (Chemenda et al., 1995; Wu et al., 2009). Under ultrahigh-temperature metamorphic conditions, the continental crust may continue, in subduction zones, to plunge into the mantle at pressures of 8–10 GPa. After that, densities of synthetic UHP metamorphic rocks of felsic composition exceed the densities of the surrounding mantle peridotites, suggesting that the continental rocks would be no longer buoyant and could continue to move down toward the mantle transition zone (Wu et al., 2009). The greater volume of UHP metamorphic rocks of continental affinity compared to the denser mafic/ultramafic rocks suggests that the buoyancy of the continental material, once detached from the subducting slab, is sufficient to transport it back to shallow crustal level (Dobrzhinetskaya and Faryad, 2011), probably in an extrusion wedge model (Massonne and Li, 2020; Zhang and Wang, 2020). However, the high-temperature metamorphic overprint exhibited by some exhumed UHP rocks suggests mantle upwelling resulting from slab breakoff during the evolution of continental crust subduction (Faryad and Cuthbert, 2020).

In this contribution, we report unprecedented data regarding Neoproterozoic coesite-forming UHPM recorded in metasedimentary rocks of the southernmost portion of the Brasília Orogen, south of the São Francisco Craton. The analyzed felsic (metasedimentary origin) and mafic high-pressure granulites comprise a thick nappe sheet in the orogenic wedge of the orogen (Fig. 1A), which is part of a nappe system that represents the southerly extension of the West Gondwana system of orogens, build by successive collisions that closed the Goiás-Pharusian Ocean in the Neoproterozoic (Ganade de Araújo et al., 2014). UHP minerals and textures were identified by combining optical petrography, Raman spectroscopy, and mineral composition. The P-T-t decompression path was tracked by Ti-in-zircon and Zr-in-rutile thermometry and U-Pb dating (LA-ICP-MS) of zircon, monazite, and rutile. Our findings, combined with literature data, allowed us to interpret that the high-pressure granulite facies metamorphism post-dates the release of the UHP rocks from the subduction channel. Once detached from the subduction channel, the coesite-bearing rock package was submitted to a partial melting process during their protracted exhumation, which was probably conducted by ductile thrust shear zones.

2. Geological setting

A protracted history of about 200 Myrs of oceanic consumption built a continuous system of orogens in the Neoproterozoic West Gondwana margin (Fig. 1A) (Bosch et al., 2011; Caby, 2003; Caby et al., 2014; Ganade de Araújo et al., 2014; Pimentel and Fuck, 1992; Triantafyllou et al., 2020). The Brasília Orogen (Fig. 1B) is part of this system and was developed during subduction-collision processes between the São Francisco, Amazonas, and Paranapanema paleoplates (Brito-Neves et al., 1999; Fuck et al., 2017; Pimentel, 2016; Valeriano, 2017; and references therein). These processes resulted in the amalgamation of the São Francisco-Paranapanema proto-continent, the first and foremost continental landmass on the western margin of Gondwana (Campos Neto et al., 2020; Caxito et al., 2022). The southernmost edge of the Brasília Orogen (Fig. 2A and B) comprises a system of flat-lying nappes, horizontally transported to ENE, obliquely to the southern margin of the São Francisco Craton.

2.1. The southernmost domain of the Brasília Orogen

From the 1980s (Trouw et al., 1986, 1983, 1980) to the regional approaches of Campos Neto and Caby (1999) and Trouw et al. (2000), five main tectonic units have been recognized along the southern extent of the Brasília Orogen (Fig. 2A), which are bounded by low angle southeast dipping thrust zones transported to E/NE. These tectonic units constitute an in-sequence nappe system (Benetti et al., 2024; Campos Neto et al., 2011; Marimon et al., 2022; Westin et al., 2021), comprised, from the inner upper (SW) to the frontal lower (NE) allochthons, of the Socorro-Guaxupé Nappe, Andrelândia Nappe System and Carrancas Nappe System. Syn-collisional flysch deposits were trapped in the intermediate and frontal nappes (Frugis et al., 2018; Kuster et al., 2020; Marimon et al., 2023; Trouw et al., 2000; Westin and Campos Neto, 2013). The inner and upper Socorro-Guaxupé Nappe pertain to the active margin of the Paranapanema upper plate, while the others have been formerly deposited on the São Francisco passive margin.

The Socorro-Guaxupé Nappe is a record of a thick magmatic arc root, recording protracted metamorphism from 790 Ma to 580 Ma (Campos Neto and Caby, 2000; Garcia and Campos Neto, 2003; Mora et al., 2014; Motta et al., 2021; Reno et al., 2009; Rocha et al., 2017; Tedeschi et al., 2018). The metamorphism registers ultra-high temperature conditions dated at ca. 625 Ma (Rocha et al., 2017). Supplementary Material 1 summarizes the published metamorphic dates for the southern Brasília Orogen. Calc-alkaline orthogneisses, charnockites, and deformed granitoids record 790–640 Ma episodic supra-subduction-related magmatism. High-K calc-alkaline granitoid record up to ca. 600 Ma syn- to late-collisional magmatism (Balis et al., 2020; Basei et al., 1995; Costa et al., 2022; Ebert et al., 1996; Gengo, 2014; Marimon et al., 2022; Mora et al., 2014; Rocha et al., 2018; Tedeschi et al., 2018; Toledo et al., 2018; Vinagre et al., 2014). Post-tectonic plutons and an A-type granitic suite intruded the exhumed lower crust around 600–575 Ma (Costa et al., 2018; Duffles et al., 2013; Janasi et al., 2009). The suture line that separates the Socorro-Guaxupé Nappe from the basement units of the passive margin (Amaral et al., 2019; Cioffi et al., 2016a, 2016b; Oliveira et al., 2019; Peternel et al., 2005; Pinheiro et al., 2019; Westin et al., 2016) and allochthons of the Andrelândia Nappe System (distal passive margin and orogenic foreland basin) is a sinuous flat-lying thrust surface transported to ENE (Fig. 2A–B).

The Andrelândia Nappe System (Fig. 2) comprises three main allochthons, which are characterized by an inverted metamorphic pattern (Motta and Moraes, 2017; Trouw et al., 2000) related to a moderate apparent thermal gradient that decreases from the upper (825 °C/GPa) to the lower (650 °C/GPa) nappes. The inverted pattern seems to have been controlled by the in-sequence thrust discontinuities from 630 Ma in the upper to 590–570 Ma in the lower allochthon (Benetti et al., 2024; Benetti, 2022; Campos Neto et al., 2011; Marimon et al., 2022; Motta and Moraes, 2017; Westin et al., 2021). The upper Três Pontas-Varginha Nappe (Campos Neto and Caby, 2000, 1999), the object of the present work, comprises an aluminosilicate-bearing granulitic package (~5 km thick), with a 130 km minimum horizontal displacement recorded by klippen structures. The prevalent rutile-kyanite-garnet-Kfeldspar gneiss occurs with (kyanite)-garnet-bearing leucogranite injections, and subordinated mafic granulites, with the

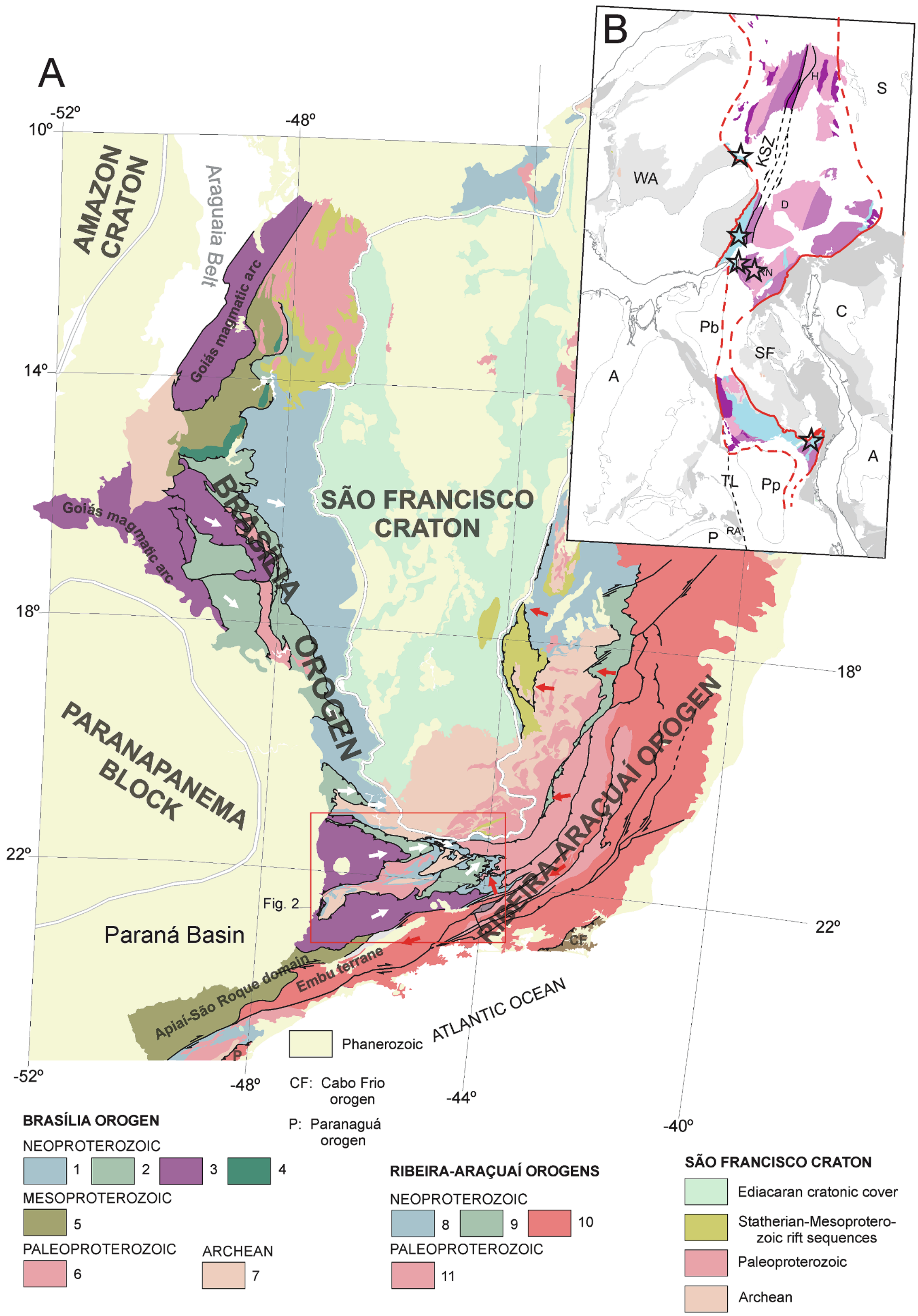

Fig. 1. (A) Simplified tectonic map (adapted from Tectonic Map of South America, Cordani and Ramos, 2016) highlighting the Neoproterozoic orogens facing the west, south, and east of São Francisco Craton. White arrows: tectonic transport of the Brasília orogen; red arrows: tectonic transport of the Ribeira-Araçauaí orogens. Brasília orogen: 1-proximal passive margin sequences; 2-distal passive margin sequence; 3-island arc and active continental margin complexes; 4-layered mafic–ultramafic complexes; 5-metasedimentary and metavolcanosedimentary sequences; 6-orthogneisses and mafic–ultramafic sequences; 7-orthogneisses and greenstone-belts. Ribeira-Araçuaí orogens: 8-rift and passive margin sequences; 9-passive margin and oceanic setting transition; 10-island arc and active continental margin complexes; 11-inlayers of orthogneisses and granulites; (B) Partial view of Western Gondwana. Cratons and covered old blocks: WA-West Africa; S-Sahara; A-Amazon; SF-São Francisco; C-Congo; A-Angola; Pb-Parnaíba; Pp-Paranapanema; P-Pampia; RA-Rio Apa. 1-cratonic covers; 2-Neoproterozoic orogens; light blue-passive margins; puple-active margin; maroon-island arc; pink-inlayers (H-Hoggar; D-Dahomei; RN-Rio Grande do Norte). Stars-coesite occurences. KSZ-Kandi shear zone; TL-Transbrasiliano Lineament.

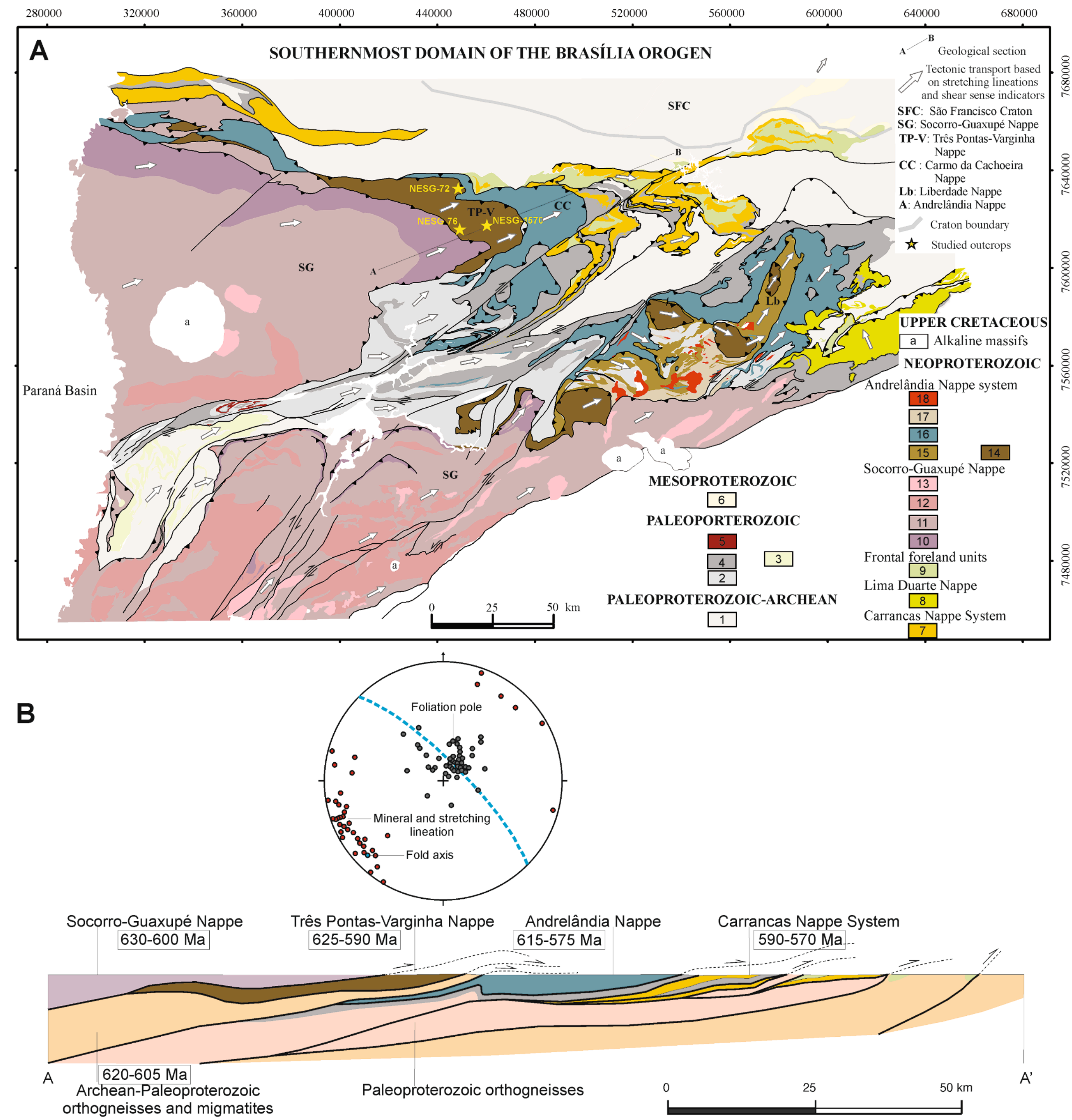

Fig. 2. (A) Geological map of the southernmost domain of the Brasília Orogen (modified after Westin et al., 2021). Paleoproterozoic-Archean: 1-orthogneisses and migmatites. Paleoproterozoic: 2-orthogneisses; 3-Immature metasedimentary sequence of São Vicente Complex and 4-Itapira Complex; 5-Statherian granite. Mesoproterozoic: 6-Carandaí and São João del Rei Groups and Itutinga Quartzite. Neoproterozoic: Psammo-pelitic passive margin sequence of 7-Carrancas Nappe System and 8-Lima Duarte Nappe; 9-Immature sequence of frontal foreland units. Socorro-Guaxupé Nappe: 10-Granulitic Complex; 11-Migmatites, diatexites, and metatexites from igneous and sedimentary protoliths; 12-Syn-to late-orogenic orthogneisses and granitoids; 13-Late-to post-orogenic granites and charnockites. Andrelândia Nappe System: 14-Três Pontas-Varginha Nappe; 15-Liberdade Nappe; 16-Andrelândia Nappe (inner foreland units); 17-Alagoa Migmatites; 18-Ms-Tur–bearing leucogranites; (B) Schematic section of the nappe stacks highlighting the main tectonic structures of the southernmost domain of the Brasília Orogen and their ages (Supplementary Material 1), as well as the equal-area stereographic lower hemisphere projection of foliation poles and stretching lineations from the Três Pontas-Varginha Nappe.

presence of immature quartzites at the base of the nappe. Silimanite-bearing assemblages prevail towards the top of the nappe. Peak metamorphic conditions at 850 °C and 15 kbar attained at about 618–605 Ma were reported in the literature (Campos Neto et al., 2010; Campos Neto and Caby, 2000; Del Lama et al., 2000; Garcia and Campos Neto, 2003; Li et al., 2021; Motta and Moraes, 2017; Reno et al., 2009; Trouw et al., 1998). Although older ages (∼650 Ma, Reno et al., 2012, 2009) and UHP metamorphic textures (Campos Neto and Caby, 2000, 1999; Li et al.,

2021) and minerals (Parkinson et al., 2001) have been reported, such extreme conditions of metamorphism remain undefined. The intermediate Liberdade Nappe corresponds to a pelitic rock package interpreted as deep-water pelagic deposits related to an accretionary wedge and distal passive margin settings (Trouw et al., 2000). Lense-shaped blocks of garnet-clinopyroxene-bearing amphibolites (retroeclogites), with omphacite relicts (Campos Neto and Caby, 1999), register eclogite metamorphic conditions of 700 °C and 17 kbar (Campos Neto and Caby, 1999; Coelho et al., 2017) at around 680–670 Ma (Campos Neto et al., 2011; Reno et al., 2009). These older ages have been interpreted as the record of the subduction-to-collision transition (Campos Neto et al., 2020; Marimon et al., 2022; Westin et al., 2021). The lower Andrelândia Nappe (Campos Neto et al., 2007; Trouw et al., 1983) is mainly composed of a thick (~850 m) and homogenous garnet-biotite-plagioclase-quartz gneiss/schist (metawacke) package. It records a rapid deposition-burial process in an orogenic foreland basin (Fontainha et al., 2021; Frugis et al., 2018; Kuster et al., 2020; Santos, 2011; Trouw, 2008) and overrides the proximal passive margin sequences (Marimon et al., 2020; Trouw et al., 2000, 1980; Westin et al., 2019; Westin and Campos Neto, 2013). The contrasting metamorphic character between the upper ultra-high-temperature Socorro-Guaxupé Nappe and the underlying high-pressure Andrelândia Nappe System underpin a subduction-collision paired metamorphic belt (e.g., Brown and Johnson, 2018).

The lower and external Carrancas Nappe system is constituted by three main tectonic discontinuities, top-to E/SE: (i) upper São Tomé das Letras Nappe; (ii) the intermediate Luminárias Nappe; and (iii) the lower Carrancas Nappe (Quéméneur et al., 2003; Trouw et al., 2002). The nappe system is characterized by a sequence of mature quartzites and grey schists up to 1 km thick and basement units (Kuster et al., 2020; Marimon et al., 2020; Westin et al., 2019, 2016; Westin and Campos Neto, 2013). The pelitic rocks vary from lower white mica-chloritoid-kyanite schist to upper white mica-garnet-staurolite-kyanite schist recording an inverted metamorphic pattern (Ribeiro and Heilbron, 1982), with metamorphic peak and nappe decompression path at ~590 Ma (Fumes et al., 2019; Westin et al., 2021, submitted). High-pressure peak metamorphic conditions of around 12–14 kbar are described for both Luminárias and Carrancas nappes (Carvalho et al., 2020; Fumes et al., 2021, 2019; Silva, 2010; Westin et al., submitted).

3. Materials and methods

Six samples representative of the Três Pontas-Varginha Nappe type-area (Fig. 2) and extracted from the top (NESG-76.6), intermediate (NESG-93A2 and NESG-1570E), and upper NESG-72 (X, Z, and U) regions of the allochthon were selected for analyses (Supplementary Material 2).

3.1. EPMA major elements analyses

Chemical analyses in garnet (Supplementary Material 3) were acquired in the Electronic Microprobe Laboratory of the NAP-Geoanalítica Core Facility of the Institute of Geosciences–USP (IGc-USP) through a JEOL JXA-8530F Field Emission Electron Probe Microanalyzer. The WDS analyses were performed under operating conditions of 2.0×10^{-8} A of current and 15 kV of accelerating voltage.

3.2. Raman spectroscopy

The Raman analyses were carried out in the Molecular Spectroscopy Laboratory of the Institute of Chemistry of the University of São Paulo (Supplementary Material 4). The analyzes were performed directly on uncoated petrographic slides using a Witec alpha 300 R Raman spectrograph equipped with a 35 mW HeNe 633 nm wavelength laser, following the procedures detailed in Martinez et al. (2021), Nobre et al. (2022, 2020) and Wang et al. (2015). Rutile diagnostic bands are found at approximately 240 cm^{-1}, 440 cm^{-1}, and 610 cm^{-1} (Frank et al., 2012; Mazza et al., 2007). Prospecting for coesite remnants began with the identification of quartz inclusions in garnets that had radial fractures. Coesite, like other silica polymorphs, has the main bands of the Raman spectrum restricted to the region <600 cm^{-1}. The main diagnostic bands for coesite, which do not mix with quartz bands, can be observed at approximately 170 cm^{-1}, 270 cm^{-1}, and 520 cm^{-1} (Hemley, 1987; Parkinson, 2000; Parkinson and Katayama, 1999).

3.3. ICP-MS trace and rare earth elements in rutile and zircon

Trace and rare earth element analyses were carried out in the Chemistry and ICP-MS Laboratory of the NAP-Geoanalítica Core Facility of the IGc-USP (Supplementary Material 5). Rutile crystals (NESG-72X) were analyzed in thin sections and zircon grains from epoxy discs (NESG-1570E). The analyses were performed with a New Wave UP-213/AF laser coupled to a Perkin Elmer/Sciex quadrupole Elan-6100/DRC ICP-MS for garnet and coupled to a ThermoScientific iCAP Q quadrupole ICP-MS for zircon and rutile analyses. The ICP-MS parameters were carrier gas flux of He and Ar of 0.48 L min^{-1}, plasma gas flux (Ar) of 16 L min^{-1}, auxiliary gas flux (Ar) of 1 L min^{-1}, and RF power of 1250 W. All results were processed through the Glitter 4.4.2 software for instrumental and fractionations corrections and the REE dataset was normalized by C1 chondrite (Sun and McDonough, 1989). Zircon spots were placed in two different zones: metamorphic overgrowths around detrital zircon and soccer ball zircon grains.

3.4. U-Pb LA-MC-ICP-MS epoxy disc analyses

U-Pb epoxy disc analyses (sample NESG-1570E) were carried out in the Geochronology Laboratory of the Geology Department of the Federal University of Ouro Preto (DEGEO–UFOP) (Supplementary Material 6). Zircon crystals were analyzed using a ThermoScientific Neptune Plus Multicollector ICP-MS coupled with a Teledyne Photon Machines G2 excimer laser. The laser parameters for analyses included a repetition rate of 6 Hz, a carrier gas flow of 0.1 L min^{-1}, fluence of 1–2 J cm^{-2}, and a spot size of 20 μm. The ICP-MS configuration included a radio frequency power of 1100 W and a make-up gas flow of 0.5 L min^{-1}. The ICP-MS is supplied with secondary electron multipliers and ion counters integrated into the Faraday cup array (Lana et al., 2017). The data acquisition followed a standard-sample-standard procedure in which 10 spots were analyzed in three different reference materials, followed by 10 spots in the unknowns, and then another block of 10 spots in the reference materials. In this case, the reference materials analyzed were the GJ-1, Plesovice (Sláma et al., 2008), and BB9 (Santos et al., 2017). Analyzes with discordance higher than 5 % were discarded. The acquired data was processed using Isoplot/Ex® 4.11 software (Ludwig, 2008), and reported errors are at 2σ level.

3.5. In-situ U-Pb LA-ICP-MS analyses

The in-situ U-Pb analyses were conducted in the ICPMS Laboratory of Géociences Montpellier (AETE-ISO regional facility of the OSU OREME) at the University of Montpellier (Supplementary Material 7). Four thin sections of granulitic gneisses (samples NESG-72X, NESG-72U, NESG-72Z, and NESG-93A2) were studied, in which zircon, monazite, and rutile crystals were analyzed (Supplementary Material 1). Scanning electron microscope (SEM) guided the LA-ICP-MS analyses. U-Pb analyses were carried out using a Compex 102 excimer laser (LambdaPhysiks) coupled to an Element XR single collector ICP-MS following the procedure described in earlier reports (e.g., Bosch et al., 2011; Bruguier et al., 2017). Zircon analyses were carried out with a spot size of 26 μm and a repetition rate of 4 Hz, monazite crystals were analyzed with a spot size of 15 μm and a repetition rate of 2–3 Hz, and rutile with a spot size of 77 μm and a repetition rate of 4 Hz. The standards used during the data acquisition were G91500 and GJ1 (zircon), Manangotry (monazite), and R10 (rutile). The acquired data was processed using Isoplot/Ex® 4.11 software (Ludwig, 2008), and reported errors are at 2σ level.

4. Results

4.1. Field relations and petrography

The paragneisses of the Três Pontas-Varginha Nappe have a high-T deformed foliation, with a NW–SE orientation, and a low-angle dip to SW. Mineral and stretched lineations (kyanite, feldspar, and quartz) trend to WSW with a low (~10°) plunge (Fig. 2B).

Feldspar-rich stretched and thinned lenses are parallel to kyanite blades (and biotite in retrograde domains) and define the main foliation (Fig. 3A). Isoclinal and intrafolial folds of feldspar-rich leucosomes are found in the lenses, with biotite-rich selvedges in the highly deformed boundaries (Fig. 3B). High-T asymmetric pressure-shadow zones (feldspar-kyanite-quartz) around garnet porphyroblasts (Fig. 3C), deflected foliation, S-C-C′ fabric, sigma-type feldspar porphyroclasts (Fig. 3D), and garnet fishes surrounded by kyanite (Fig. 3E) indicate top-to-the-ENE/NE sense of shear. The foliation is cylindrically folded as a gentle synform with the hinge line plunging to SW (Fig. 2B), defining the spoon-like shape of the nappe. The asymmetric east-verging folds were later deformed by antithetic normal faults (Fig. 3F).

The predominant lithotype is a light grey to bluish coarse-grained porphyroblastic rutile-kyanite-garnet-quartz-feldspar gneiss (Fig. 3A; samples NESG-72C, NESG-72X, NESG-76.6 and NESG-1550). The primary assemblage comprises kyanite, garnet, mesoperthite, quartz,

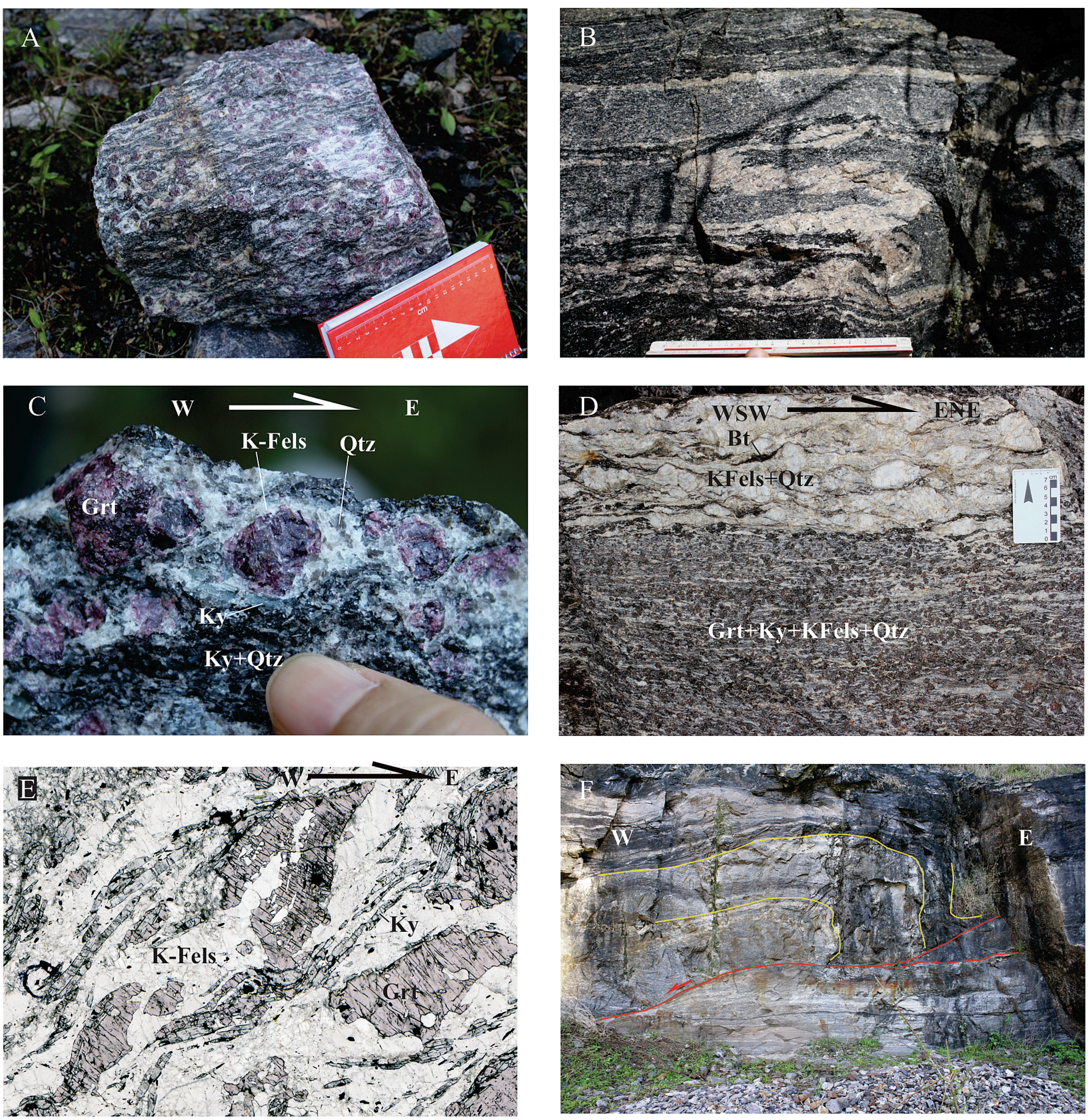

Fig. 3. Outcrops NESG-72 (A, B, C, E, and F) and NESG-1570 (D): (A) Predominant kyanite-garnet-K-feldspar granulite; (B) Passive folds of *syn*-foliation K-feldspar-rich leucosomes; (C) Garnet asymmetrically armored by felsic phases (K-feldspar, quartz), and wrapped by the foliation. Top-to-the-E shearing; (D) Deformed garnet-kyanite-K feldspar gneiss with coarse-grained quartz-feldspar band. Top-to-the-ENE shearing; (E) Skeletal garnet fish wrapped by kyanite-bearing foliation. Top-to-the-E shearing; (F) East-verging asymmetrical fold cut by late antithetic shear zone.

rutile, and, locally, some white mica (Fig. 3A–B). Microcline, biotite, ilmenite, and plagioclase occur as retrograde phases, and zircon, monazite, and apatite are the main accessory minerals. Garnet occurs as fractured idioblastic/subidioblastic to xenoblastic porphyroblasts of up to 1.5 cm in diameter (Fig. 3A–B and 4A–B). Some of the porphyroblasts exhibit textural zoning defined by an inter-kinematic core with rutile and ilmenite inclusion trails wrapped by amoeboid-shaped quartz and microcline (Fig. 4B). The ameboid-shaped inclusions separate the core from the garnet mantle, characterized by misoriented rutile-ilmenite and biotite inclusions, and from the inclusion-free rim (Fig. 4B). Garnet porphyroblasts of the analyzed gneisses are commonly fractured around inclusions of different mineral phases. Some of the fractures present a radial pattern, usually crosscutting other fractures and related to round or irregular-shaped quartz crystals (Fig. 4E). These radial fractures are usually found in the edges of the garnet crystals, although they are also found in the center of larger porphyroblasts. Outer quartz rings around one or more quartz crystals with ovoid shapes are common, although a clear palisade texture (Chopin, 1984; Schertl et al., 1991) was not observed.

Garnet porphyroblasts are often asymmetrically armored by neosome lenses (Fig. 3B) and occur as asymmetrical and skeletal fish crystals in a meter-thick shear zone. Kyanite crystals are subidioblastic, oriented according to the main foliation (Fig. 4A–B), with inclusions of rutile, quartz, ilmenite, and zircon. Rutile occurs as coarse-grained and needle inclusions in garnet and kyanite (Fig. 4A–C) and as brownish baguettes in the matrix, locally wrapped by ilmenite. Typical hat-shaped zircon grains were observed in contact with rutile crystals (Fig. 4G–H). Intergranular sillimanite is pervasive in these rocks, although higher proportions of sillimanite occur towards the top of the nappe. These sillimanite-bearing gneisses (NESG-93A2 and NESG-1570) have higher contents of biotite and lesser contents of kyanite (Fig. 4C), with prismatic crystals and fine-grained acicular aglomerates (fibrolite) of sillimanite oriented according to the main foliation. Sillimanite inclusions in the rims and around garnet porphyroblasts are also found, and fibrolite partially replaces kyanite and occurs with biotite.

White-colored quartz-feldspar neosomes occur as centimetric lenses with irregular shapes within the foliation interconnected with veins in a dilational metatexite migmatite (Fig. 3A). They have a coarse-grained granoblastic texture with lesser amounts of biotite, garnet, kyanite, rutile, zircon, and monazite. Garnet-rich mesocratic boudins also occur as high-density residues wrapped by thin leucosome lenses.

Subordinate grey to dark-green-colored rutile-titanite-hornblende-garnet gneiss occurs as metric-sized lenses containing garnet, hornblende, plagioclase, quartz, titanite, rutile, and minor clinopyroxene (NESG-72U; Fig. 4D and 4F). Quartz + plagioclase leucosomes occur as continuous lenses with lobate grain boundaries that trap hornblende-rich oriented blades and involve garnet crystals (Fig. 4D). Titanite and rutile occur in the quartz-feldspathic groundmass and as inclusions in garnet (Fig. 4D). Radial fractures in garnet crystals around rounded quartz inclusions (Fig. 4F) and needle-shaped rutile inclusions are also common in this mafic lithotype.

The main rutile-kyanite-garnet-quartz-feldspar gneiss has a pervasive foliation delineated by quartz, feldspar, and kyanite shape fabric (Fig. 4A–B), which may contain intrafolial discontinuous passive folds of quartz-feldspar stretched lenses (Fig. 3C). Mineral (kyanite, rutile, K-feldspar) and stretched lineations are W-SW plunging and kinematic indicators (e.g. sigmoidal S-shear fabric, winged feldspar sigma-type porphyroclasts, shear-band boudins, mineral fishes) show a top-to-the ENE sense of movement. The layered neosome outlines E-verging asymmetrical folds (Fig. 3D). High-grade ductile shear microstructures, often related to top-to-east displacement, are common features throughout the allochthon. Stair-stepping asymmetrical mantled porphyroclasts of microcline and quartz occur associated with an asymmetric distribution of myrmekites and plastically deformed mesoperthite. Garnet, plagioclase, clinopyroxene, and hornblende fishes are found in elongated coarse-grained quartz ribbons of both rutile-kyanite-garnet-quartz-feldspar and rutile-titanite-hornblende-garnet gneisses (Campos Neto and Caby, 2000; Trouw et al., 2000). Skeletal garnet fishes also occur with elongate S-shaped quartz in a sillimanite-rich mylonytic band. Biotite-rich asymmetrical pressure shadow zones in garnet porphyroclast are common within mylonitic bands.

4.2. Garnet composition

Garnet porphyroblasts of the rutile-kyanite-garnet-quartz-feldspar gneiss (sample NESG-72X) have major element composition compatible with garnet crystals generated during granulite facies metamorphism (Fig. 5A; Schönig et al., 2021), with $X_{Alm} + X_{Sps}$ between 0.75 and 0.79, X_{Grs} lower than 0.04, and X_{Prp} between 0.19 and 0.20 (Fig. 5A). A garnet porphyroblasts with a core with lobate edges wrapped by a strain cap overgrowth were observed. The core has a concentric chemical zoning, with enrichment in X_{Prp} compensated by the decrease in X_{Grs} and X_{Sps}, from the inner to the outer zone (Fig. 5B). X_{Alm} has similar values throughout the core. The strain cap is enriched in X_{Grs} and depleted in X_{Alm} and X_{Sps}, in comparison with the outer zone of the garnet core, with similar X_{Prp} values.

The analyzed garnet porphyroblast of the sillimanite-bearing gneiss (NESG-1570) has higher values of X_{Prp} (0.28–0.41), lower $X_{Alm+Sps}$ (0.51–0.63) and intermediate values of X_{Grs} (0.05–0.20) when compared to sample NESG-72X (Fig. 5A). Spot analyzes with X_{Grs} higher than 0.12 (Supplementary Material 3 – spots 6, 8, 12, 19, and 20) are classified as eclogite/ultra-high-pressure facies crystals, while X_{Grs} lower than 0.09 are compatible with granulite facies crystals (Fig. 5A). A negative correlation is observed between X_{Grs} and X_{Prp}, with the higher X_{Grs} values accompanied by the lower X_{Prp} contents (<0.36), with no clear correlation with X_{Alm} and X_{Sps} values (Fig. 5C).

Xenomorphic garnet porphyroblasts involved in granoblastic plagioclase (andesine) crystals of a rutile-titanite-hornblende-garnet gneiss with clinopyroxene (NESG-72U) have major element composition similar to that of eclogite/ultra-high-pressure metamorphic conditions (Fig. 5A). These crystals have higher X_{Grs} (0.21–0.36) and lower $X_{Alm} + X_{Sps}$ (0.48–0.60) when compared to the garnet porphyroblasts of samples NESG-72X and NESG 72U, with X_{Prp} (0.15–0.27) values similar to the obtained for the NESG-72X sample (Fig. 5B). X_{Alm} has a negative correlation with X_{Grs} and X_{Sps} and a positive correlation with X_{Prp} (Fig. 5C).

4.3. Rutile needle-shaped inclusions in garnet

Oriented needle-shaped inclusions of (Fe)-Ti-O minerals, with subordinate Si-O minerals, were observed in both rutile-titanite-hornblende-garnet (NESG-72U – Fig. 6A) and rutile-kyanite-garnet-quartz-feldspar (NESG-72X and NESG-72C – Fig. 6B–C) gneisses. The needles are thin rectangular rod-shaped, of varying lengths (up to 300 μm), displaying a disposition that seems to be conditioned by the garnet host, forming a network with angles of 60° (Fig. 6A–C). Raman spectroscopy mapping of a needle-shaped inclusion has rutile diagnostic bands (Frank et al., 2012; Mazza et al., 2007) at approximately 240 cm^{-1}, 440 cm^{-1}, and 610 cm^{-1} (Fig. 6D–E).

4.4. Coesite remnants in garnet

Reflected light microscopy and Raman spectroscopy mapping of quartz inclusions associated with radial fractures in garnet highlight the presence of ~1.5–3.0 μm coesite remnants in both rutile-kyanite-garnet-quartz-feldspar (NESG-76.6) and rutile-titanite-hornblende-garnet (NESG-72U) gneisses (Fig. 7A–D). The Raman spectra of the remnants have the main diagnostic bands for coesite (Hemley, 1987; Parkinson, 2000; Parkinson and Katayama, 1999) at approximately 170 cm^{-1}, 270 cm^{-1}, and 520 cm^{-1} (Fig. 7E), which are not observed in the Raman spectra of quartz. Additionally, two generations of quartz were identified: (i) Qz-1: characterized by its lower relief and lower fluorescence;

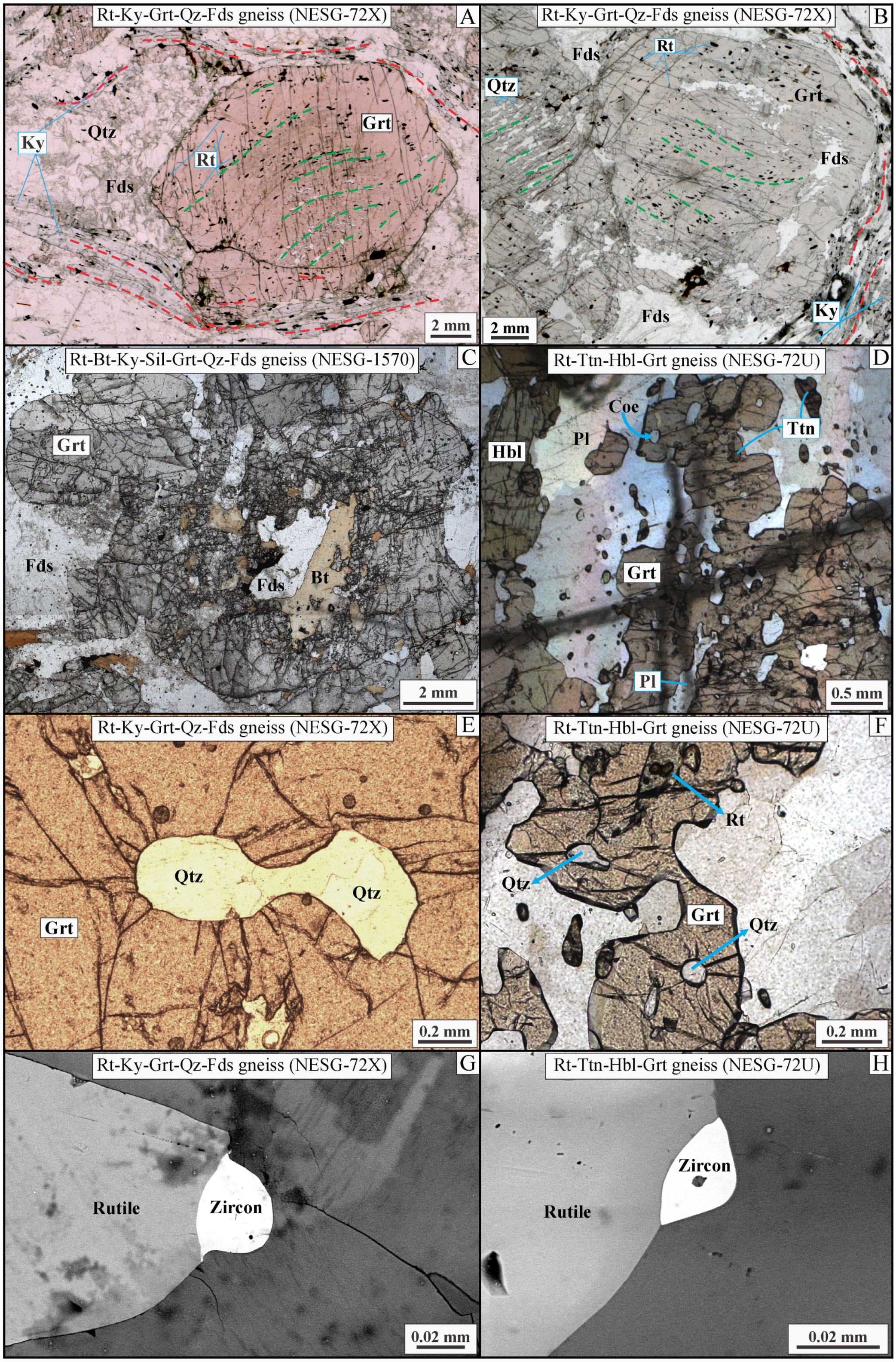

Fig. 4. (A) and (B) Photomicrographs of the analyzed rutile-kyanite-garnet-quartz-feldspar gneiss (NESG-72X). Emphasis on the idioblastic to subidioblastic garnet porphyroblasts and oriented and deformed kyanite crystals. Green dashed lines mark the internal foliation defined by mineral inclusions in garnet, while the red continuous lines mark the main foliation of the rock; (C) Photomicrograph of a rutile-biotite-kyanite-sillimanite-garnet-quartz-feldspar gneiss (NESG-1570) highlighting a xenoblastic garnet porphyroblast; (D) photomicrograph of the analyzed rutile-titanite-hornblende-garnet gneiss. Highlight for the localization of the coesite remnant identified in this rock (see Section 4.4); Radial fractures around ameboid-shaped quartz inclusions in a garnet porphyroblast of samples NESG-72X (E) and NESG-72U (F); SEM images of hat-shaped zircon crystals associated with rutile in the matrix of samples NESG-72X (G) and NESG-72U (H). Mineral abbreviations after Warr (2021).

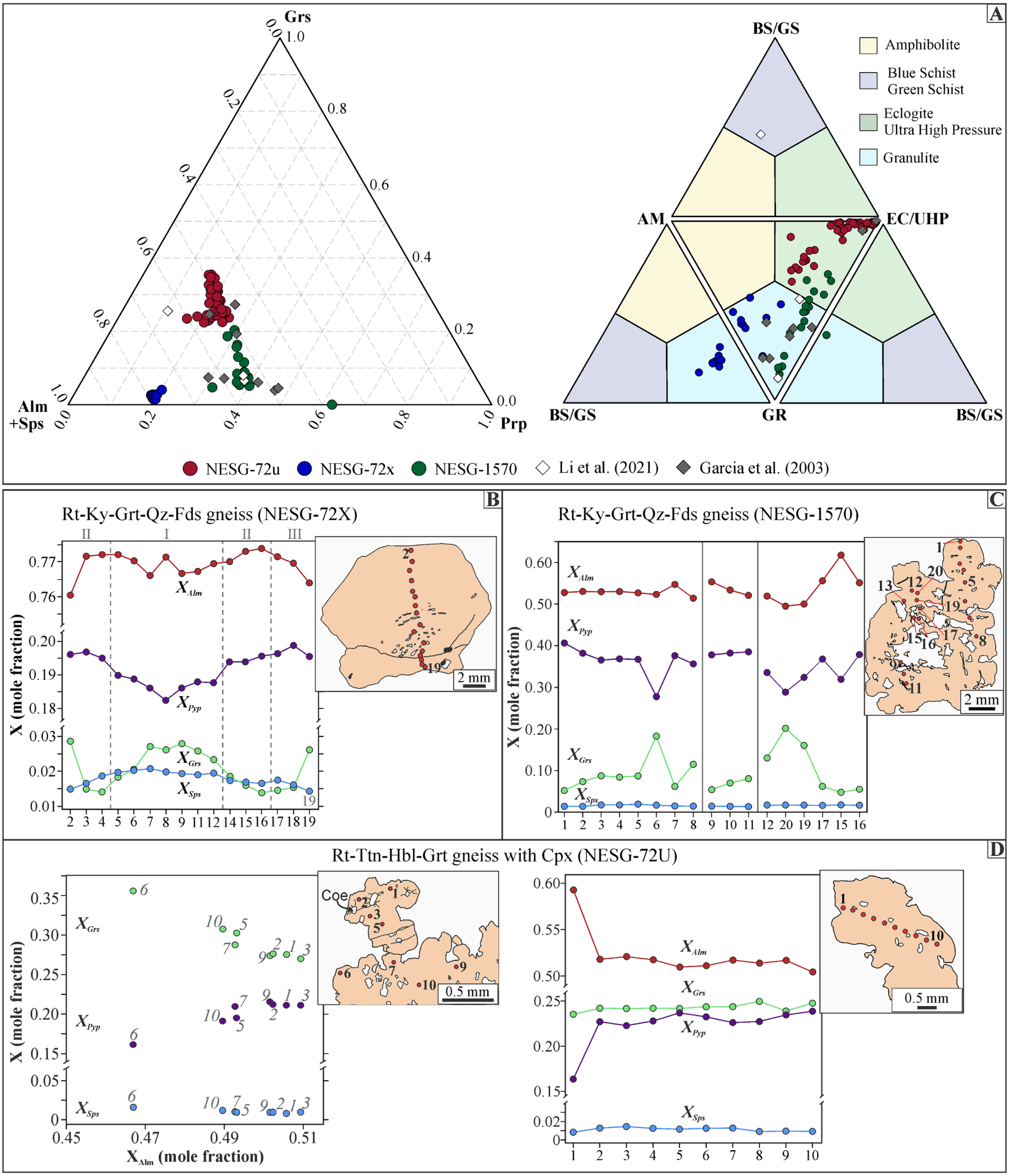

Fig. 5. (A) EPMA data of the analyzed garnet porphyroblasts plotted in ternary diagrams of garnet composition (Grs: grossular; Alm: almandine; Sps: spessartine; Prp: pyrope) generated with MinPlot (Walters, 2022) and metamorphic facies (MORB composition – Bucher and Frey, 2002) plotted with garnetRF v1.1 (Schönig et al., 2021); (B–D) Garnet end-members composition of the analyzed garnet porphyroblasts. X_{Alm} = (Alm/Alm + Prp + Sps + Grs), X_{Prp} = (Prp/Alm + Prp + Sps + Grs), X_{Sps} = (Sps/Alm + Prp + Sps + Grs) and X_{Grs} = (Grs/Alm + Prp + Sps + Grs) in moles. The calculation considered Fe as FeO^{Total}.

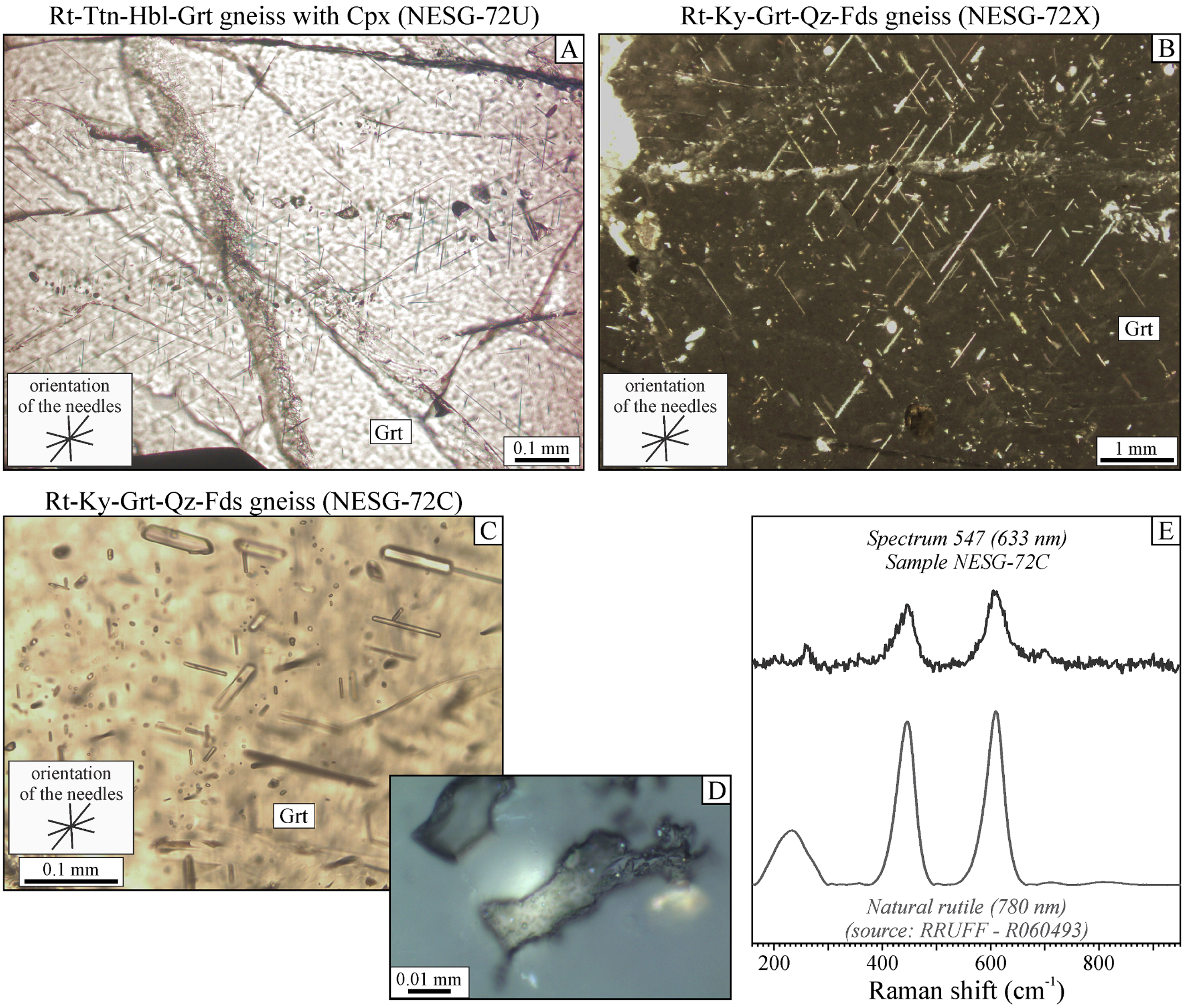

Fig. 6. Quartz and rutile needle inclusions in both (A) rutile-titanite-hornblende-garnet (NESG-72U) and (B) and (C) rutile-kyanite-garnet-quartz-feldspar (NESG-72X and NESG-72C) gneisses. Note the network with angles of 60° formed by the needles; (D) Reflected light image highlighting the presence of rutile among the needle inclusions in sample NESG-72C; (E) Raman spectrum of the analyzed needle inclusion showing the diagnostic bands of rutile around 240 cm^{-1}, 440 cm^{-1} and 610 cm^{-1}. A Raman spectrum of natural rutile of the RRUFF™ Project was inserted for comparison. Mineral abbreviations after Warr (2021).

(ii) Qz-2: with higher relief and fluorescence (Fig. 7B and 7D). The coesite remnants have intermediate relief when compared to Qz-1 and Qz-2 and were found within the Qz-1 crystals (Fig. 7B and 7D).

4.5. Zircon: U-Pb dating, REE composition, and Ti-in-zircon thermometry

4.5.1. Hand-picked zircon crystals of the sillimanite-bearing gneiss (NESG-1570)

Three distinctive morphological groups were identified in the rutile-biotite-kyanite-sillimanite-garnet-quartz-feldspar gneiss (Supplementary Material 6). The first corresponds to prismatic and anhedral zircon cores, mostly with oscillatory growth zoning. The second is soccer ball crystals (predominant group) – characterized by multifaceted grains with intermediate luminescence and grey zoning, which occurs as individual grains or as overgrowths over inherited cores. The third group comprises zircon overgrowths (subordinated group) – crystals with lower luminescence and isometric texture surrounding prismatic grains. Considering the admitted sedimentary origin for the protolith, the high-temperature metamorphism that affected the analyzed rocks, and the described morphological types/growth zoning, the first group is considered detrital. In contrast, the second and third are considered metamorphic crystals. Therefore, REE, Ti-in-zircon, and U-Pb analyses were restricted to soccer ball crystals and metamorphic overgrowths.

Soccer ball crystals have $^{206}Pb/^{238}U$ dates ranging from 702 Ma to 607 Ma ($n = 15$; 2σ errors = 15–20), with thirteen analyses defining a weighted average age of 624 ± 7 Ma (MSWD = 2.0) (Fig. 8A). The metamorphic overgrowths have dates ranging from 677 Ma to 608 Ma ($n = 13$; 2σ errors = 15–20), with a weighted average age of 620 ± 5 Ma (MSWD = 1.2) defined by eleven analyzes (Fig. 8A). Since both weighted average ages overlap within errors, the twenty-four analyses have been pooled and provided a concordia age of 622 ± 4 Ma (MSWD = 0.54), considered the most reliable age for the metamorphic overgrowths and soccer-ball grains (Fig. 8A).

Zircon REE contents are distinguishable between soccer ball crystals and metamorphic overgrowths around prismatic grains (Fig. 9A). Although all analyzed crystals display slightly HREE richer patterns with

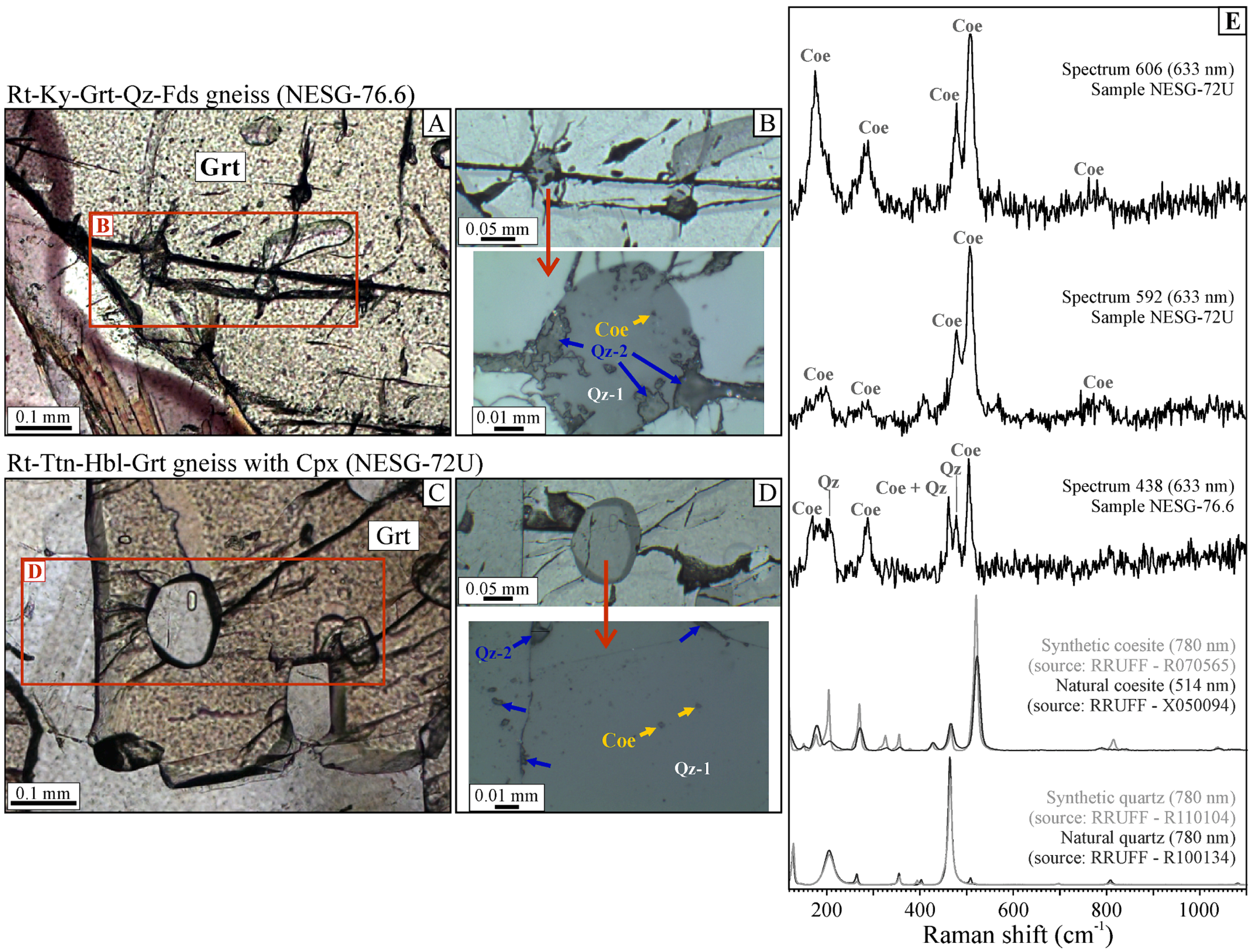

Fig. 7. Quartz inclusions in garnet porphyroblasts associated with radial fractures of both rutile-kyanite-garnet-quartz-feldspar (NESG-76.6) and rutile-titanite-hornblende-garnet with clinopyroxene (NESG-72U) gneisses. (A) and (C): photomicrographs highlighting the radial-pattern fractures around quartz inclusions; (B) and (D) reflected light images highlighting quartz-1 (Qz-1), quartz-2 (Qz-2), and coesite (Coe) remnants in the analyzed inclusions; (E) Raman spectra of the analyzed remnants showing the diagnostic bands of coesite indicated by the abbreviation Coe. Synthetic and natural coesite and quartz Raman spectra of the RRUFF™ Project were inserted for comparison. Mineral abbreviations after Warr (2021).

negative Eu anomalies, soccer ball crystals are poorer in REE content and tend to exhibit flatter patterns in the HREE than the metamorphic overgrowths.

Soccer ball crystals yielded Ti concentrations between 5.1 ppm and 15.1 ppm (n = 11), yielding temperatures (Watson et al., 2006) between 685 °C and 778 °C (errors = 11–13). Younger crystals tend to yield higher temperatures, although individual data are similar within error (Fig. 9B). Metamorphic overgrowths around prismatic detrital cores have Ti concentrations ranging from 10.6 ppm to 20.8 ppm (n = 3), which register temperatures from 746 °C to 809 °C (errors = 12–13) (Fig. 9B).

4.5.2. U-Pb in situ dating (thin section)

The zircons of the rutile-kyanite-garnet-quartz-feldspar gneiss (NESG-72X) provided a complex distribution, probably due to abundant inherited detrital grains from the sedimentary protolith. $^{206}Pb/^{238}U$ dates range from 1010 Ma to 556 Ma (n = 27; 2σ errors = 12–40), with eight concordant dates of 1010 ± 25 Ma, 769 ± 22, 700 ± 20 Ma, 698 ± 20 Ma, 659 ± 24 Ma, 624 ± 29, 592 ± 20 Ma and 563 ± 35 Ma (Supplementary Material 7; Fig. 8B). The zircon inclusions in garnet yielded concordant dates between 1010 Ma and 624 Ma, whereas matrix crystals yielded concordant dates between 769 Ma and 592 Ma.

Zircon grains found as inclusions in garnet or in the matrix of the rutile-titanite-hornblende-garnet gneiss (NESG-72U) plot either concordantly at around 590 Ma (n = 7; 2σ errors = 16–46) or on a mixing line between a radiogenic and common lead end-member (Fig. 8B). All the results combined yielded a lower intercept age of 594 ± 5 Ma (n = 29; MSWD = 0.78).

Zircon crystals found in the matrix of the kyanite-quartz-feldspar neosome (NESG-72Z) define a Discordia line with upper and lower intercepts at 2094 ± 58 Ma and 587 ± 26 Ma (n = 22; MSWD = 1.6) (Fig. 8B). Although the upper intercept is loosely defined, the distribution of the data points indicates that the studied rock contains Paleoproterozoic zircons that were affected by a thermal event of ca. 590 Ma.

4.6. Rutile: U-Pb in situ dating and Zr-in-rutile thermometry

Most of the analyzed rutile grains of both samples of the rutile-kyanite-garnet-quartz-feldspar gneiss come from the matrix. All acquired data are either concordant at around 590–600 Ma (Supplementary Material 7; 2σ errors = 16–59) or plot on the right side of the Concordia line, a location typically ascribed to the incorporation of common Pb in the analyses. Twenty-six dates of sample NESG-72X define a lower intercept age of 586 ± 5 Ma (n = 26; MSWD = 1.01),

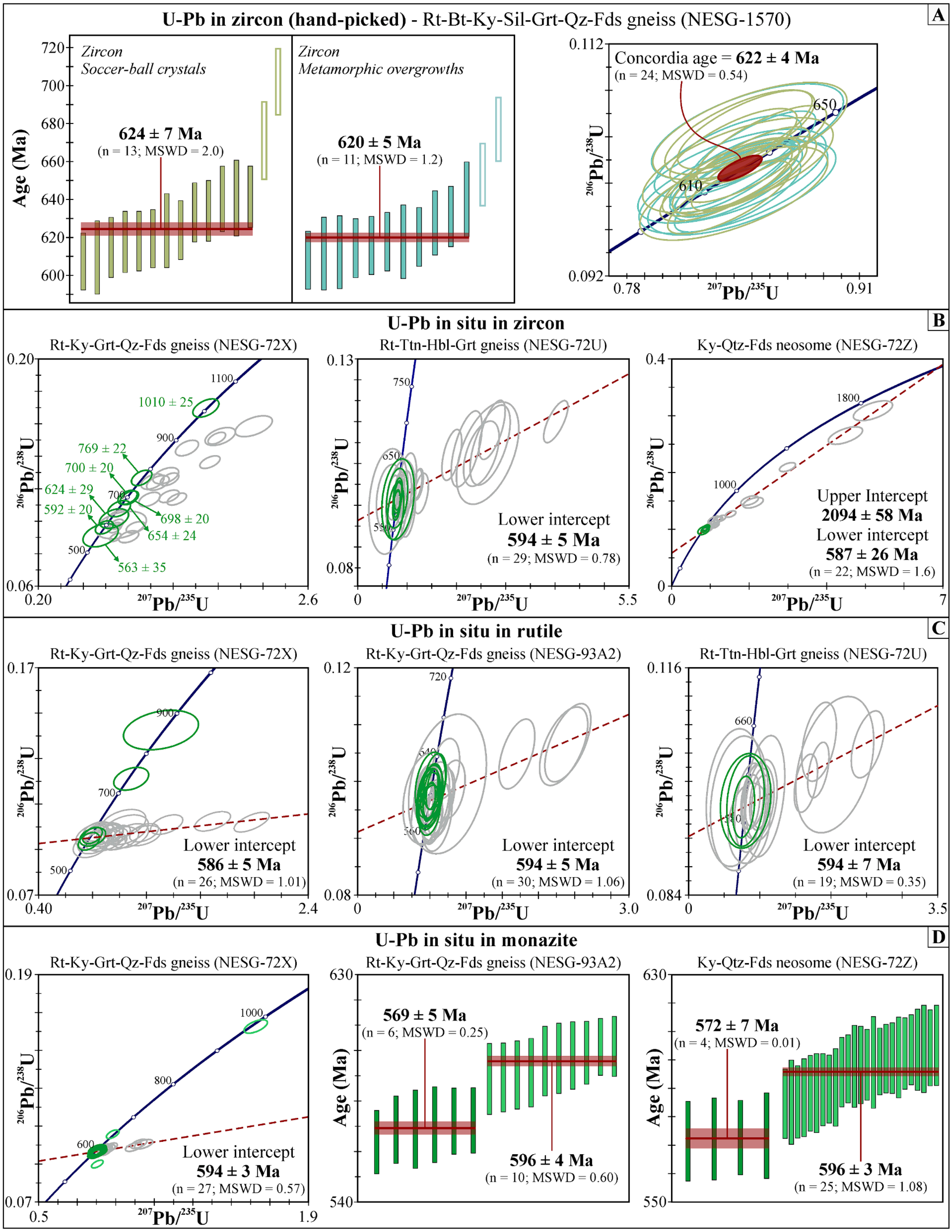

Fig. 8. (A) U-Pb weighted average graphs and Concordia diagram for hand-picked zircons from the rutile-biotite-kyanite-sillimanite-garnet-quartz-feldspar gneiss (NESG-1570); (B) In situ dates displayed in U-Pb Concordia diagrams for zircons from the rutile-kyanite-garnet-quartz-feldspar (NESG-72X), rutile-titanite-hornblende-garnet (NESG-72U) gneisses and kyanite-quartz-feldspar neosome (NESG-72Z); (C) In situ dates displayed in U-Pb Concordia diagrams for rutile crystals from the rutile-kyanite-garnet-quartz-feldspar (NESG-72X and NESG-93A2) and rutile-titanite-hornblende-garnet (NESG-72U) gneisses. The acquired ages are similar independently of the lithotype and microstructural site.; (D) In situ dates displayed in U-Pb Concordia diagram and weighted average graphs for monazite crystals from the rutile-kyanite-garnet-quartz-feldspar gneiss (NESG-72X and NESG-93A2) and kyanite-quartz-feldspar neosome (NESG-72Z). Green ellipses correspond to dates with discordance equal or lower to 10% (concordant), while grey ellipses correspond to dates with discordance higher than 10% (discordant). Mineral abbreviations after (Warr, 2021).

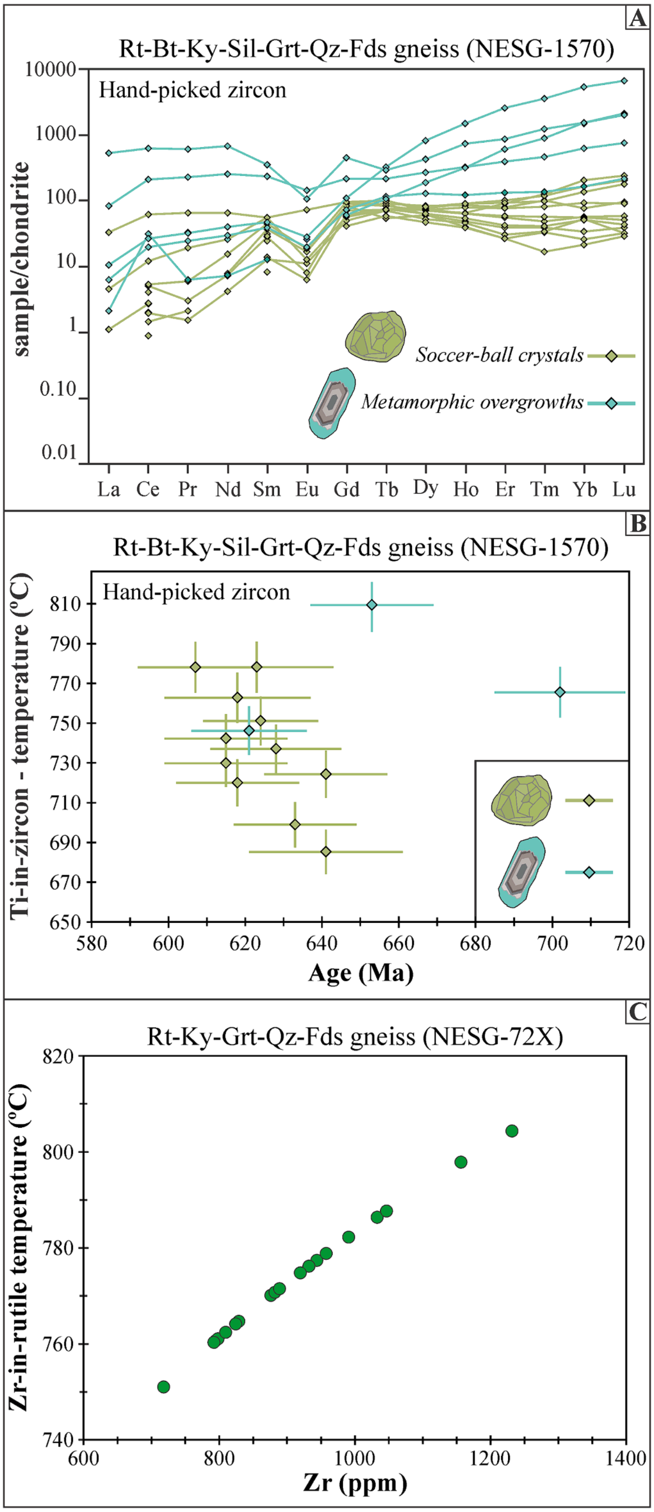

Fig. 9. (A) REE spider diagram for hand-picked zircons from the rutile-biotite-kyanite-sillimanite-garnet-quartz-feldspar gneiss (NESG-1570); (B) Age (Ma) vs. Ti-in-zircon temperature (°C) graph for hand-picked zircons from the rutile-biotite-kyanite-sillimanite-garnet-quartz-feldspar gneiss (NESG-1570); (C) Zr (ppm) vs. Ti-in-zircon temperature (°C) for rutile crystals from the rutile-kyanite-garnet-quartz-feldspar gneiss (NESG-72X). Mineral abbreviations after Warr (2021).

besides two significantly and concordant older matrix grains of 859 ± 40 Ma and 737 ± 24 Ma (Fig. 8C). Sample NESG-93A2 dates define a regression line with a lower intercept at 594 ± 5 Ma (n = 30; MSWD = 1.06) (Fig. 8C). The dates obtained for rutile crystals of the rutile-titanite-hornblende-garnet gneiss (NESG-72U) are similar to the obtained for sample NESG-93A2, with a regression line defining a lower intercept age of 594 ± 7 Ma (n = 19; MSWD = 0.35) (Fig. 8C).

The Zr concentration of rutile grains from sample rutile-kyanite-garnet-quartz-feldspar gneiss (NESG-72X) varies between 718.0 ppm and 1231.5 ppm (n = 22), with no distinction between inclusions and matrix grains. Calculated temperatures (β-quartz stability field; Tomkins et al., 2007) considering a metamorphic peak pressure of 15 kbar (Campos Neto and Caby, 2000; Garcia and Campos Neto, 2003; Reno et al., 2009) range from 751 °C to 804 °C (Fig. 9C).

4.7. *Monazite: U-pb in situ dating*

Monazite crystals found as inclusions in garnet and in the matrix of two samples of the rutile-kyanite-garnet-quartz-feldspar gneiss were analyzed (Supplementary Material 7). Since there is no clear correlation between texture relations and acquired dates, the analyses were not treated separately. The majority of the monazite dates obtained in sample NESG-72X plot concordantly at around 600 Ma (n = 27; 2σ errors = 10–14) or on the right of the Concordia curve, suggesting the presence of common lead in the analyzed crystals (Fig. 8D). These dates define a Discordia line with a lower intercept at 594 ± 3 Ma (MSWD = 0.57) interpreted as the age of the main monazite growth (Fig. 8D). Three analyses are exceptions to the main group, two concordant of 648 ± 11 Ma (Supplementary Material 7; fb_19) and 972 ± 16 (Supplementary Material 7; fb_20) Ma and one discordant of 556 ± 10 Ma (Supplementary Material 7; fb_8). The dates of sample NESG-93A2 plot concordantly between 610 Ma and 560 Ma (n = 20; 2σ errors = 10–20), comprising two distinct age groups of 596 ± 4 Ma (n = 10; MSWD = 0.60) and 569 ± 5 Ma (n = 6; MSWD = 0.25) (Fig. 8D). The ~ 596 Ma population is similar within errors to the lower intercept age of sample NESG-72X.

The distribution of the monazite dates of the kyanite-quartz-feldspar neosome (NESG-72Z) is similar to that observed for sample NESG-92A2. The dates set varies between 605 Ma and 571 Ma (n = 29; 2σ errors = 12–16), comprising two main age groups of 596 ± 3 Ma (n = 25; MSWD = 1.08) and 572 ± 7 Ma (n = 4; MSWD = 0.01) (Fig. 8D). The four dates of the younger age were obtained in one grain located within a biotite-rich lens of the sample. Both age groups are similar, within error, to the age groups yielded by sample NESG-92A2.

5. Discussion

5.1. *Tracing ultrahigh-pressure metamorphic conditions*

The high-pressure (sillimanite)-kyanite-garnet-Kfeldspar and Pl-bearing gneisses of the Três Pontas-Varginha Nappe display garnet porphyroblasts with core-mantle-rim grow textures that evince inter-tectonic core and a syn- to late-kinematic mantle-rim (Fig. 4A–B). Texturally homogeneous and extensively consumed garnet porphyroblasts, wrapped and invaded by quartz-plagioclase probably from the melt phase, are also present (Fig. 4C–D). Chemical analyses indicate chemical zoning in garnet porphyroblasts of both rutile-kyanite-garnet-quartz-feldspar (NESG-72X) and rutile-titanite-hornblende-garnet (NESG-72U) gneisses (Fig. 5B and 5D), with a clear end-member chemical zoning identified in sample NESG-72X (Fig. 5B). The chemical composition of the garnet porphyroblasts of the rutile-titanite-hornblende-garnet gneiss are compatible with growing under eclogite/ultra-high-pressure metamorphic conditions (Fig. 5A), which are also recorded by garnet porphyroblasts of the rutile-biotite-kyanite-sillimanite-garnet-quartz-feldspar gneiss (NESG-1570).

Radial fractures around round-shaped polycrystalline quartz inclusions (Figs. 4E–F and 7) and 60° angled networks of needle-shaped rutile crystals (Fig. 6) within garnet porphyroblasts point to ultra-high pressure metamorphic conditions. These extreme metamorphic conditions are confirmed by the presence of coesite microinclusions within the polycrystalline quartz inclusions of both rutile-kyanite-garnet-quartz-feldspar (NESG-76.6) and rutile-titanite-hornblende-garnet (NESG-72U) gneisses (Fig. 7A–D). The radial fractures in garnet around quartz inclusions are a widely reported microstructure for UHP metamorphic rocks (Brown and Johnson, 2018; Whitney et al., 2000) and are interpreted as the result of polymorph positive-volume expansion transformation from coesite to α-quartz during decompression (Gillet et al., 1984). Rutile needle-shaped inclusions in garnet, oriented in a network with angles of 60°, have been reported for (U)HP, (U)HT, and mantle-derived rocks (Ague and Eckert, 2012; Alifirova et al., 2015, 2012; Griffin et al., 1971; Hwang et al., 2007; Mposkos and Kostopoulos, 2001; Ye et al., 2000). Hwang et al. (2007) proposed that generating needle-like inclusions in garnet, mainly rutile, might be controlled by a metasomatic dissolution-reprecipitation mechanism in the presence of a fluid phase under UHP conditions. The titanium in garnet at UHP conditions, generally in the presence of clinopyroxene, may exsolve during decompression (Axler and Ague, 2015; Zhang et al., 2003), and the shape-preferred orientation of the needle inclusions, parallel to ⟨1 1 1⟩ garnet, connecting the octahedral garnet sites to the inclusions directions corroborates the reprecipitation hypothesis (Keller and Ague, 2020). Needle-like inclusions are also reported for lower metamorphic-grade rocks, however, they are smaller, rarer, and randomly oriented (Ague and Eckert, 2012). Additionally, some of the analyzed garnet porphyroblasts have Ti-rich domains (TiO_2 = 0.10–0.16 wt%) comparable to garnets with diamond inclusions from the Edough Massif (Caby et al., 2014), which also supports the dissolution-reprecipitation mechanism (Supplementary Material 3, also reported by Garcia and Campos Neto, 2003, and Li et al., 2021).

5.2. Decompression path from high-pressure granulite facies conditions

Granulite facies peak metamorphic conditions of 800–850 °C and 1.3–1.6 GPa were estimated for the rutile-kyanite-garnet granulites from the Três Ponta-Varginha Nappe, through classical geothermobarometric methods (Campos Neto et al., 2010; Campos Neto and Caby, 2000, 1999; Del Lama et al., 2000; Garcia and Campos Neto, 2003; Motta and Moraes, 2017; Trouw et al., 1998) and thermodynamic modeling (Li et al., 2021; Reno et al., 2009). Decompression paths from 1.45 GPa at 850 °C until around 0.7 GPa at 650 °C, compatible with a tectonic unroof of about 25 km of lithostatic load (continental crust density ~2850 kg/cm^3 – Dziewonski and Anderson, 1981), were also estimated by these authors (Fig. 10).

These granulite facies metamorphic conditions are recorded mainly by the chemical composition of the garnet porphyroblasts from the rutile-kyanite-garnet-quartz-feldspar gneiss (NESG-72X), although similar results were obtained for crystals from the rutile-biotite-kyanite-sillimanite-garnet-quartz-feldspar gneiss (NESG-1570) (Fig. 5A). Similar compositions were also reported by Garcia and Campos Neto (2003) and Li et al. (2021) (Fig. 5A). The granulite facies high temperatures are also recorded by rutile crystals from the kyanite-bearing gneisses (NESG-72X), which yielded Zr-in-rutile temperatures (Tomkins et al., 2007; β-quartz field) between 750 °C and 805 °C (at 1.5 GPa) (Fig. 9C), within the peak metamorphic conditions reported in the literature, and similar to the Ti-in-Zr temperatures reported by Reno et al. (2009).

REE patterns of hand-picked soccer ball-type and metamorphic overgrowths zircon crystals from the rutile-biotite-kyanite-sillimanite-garnet-quartz-feldspar gneiss (NESG1570) are enriched in HREE and have negative Eu anomalies, although the soccer ball crystals tend to have lower REE contents and flatter HREE patterns (Fig. 9A). The soccer ball zircon typology (Supplementary Material 6) is reckoned to grow under granulite facies metamorphic conditions (Hoskin and Schaltegger, 2003; Vavra et al., 1999), and the negative Eu anomalies are commonly

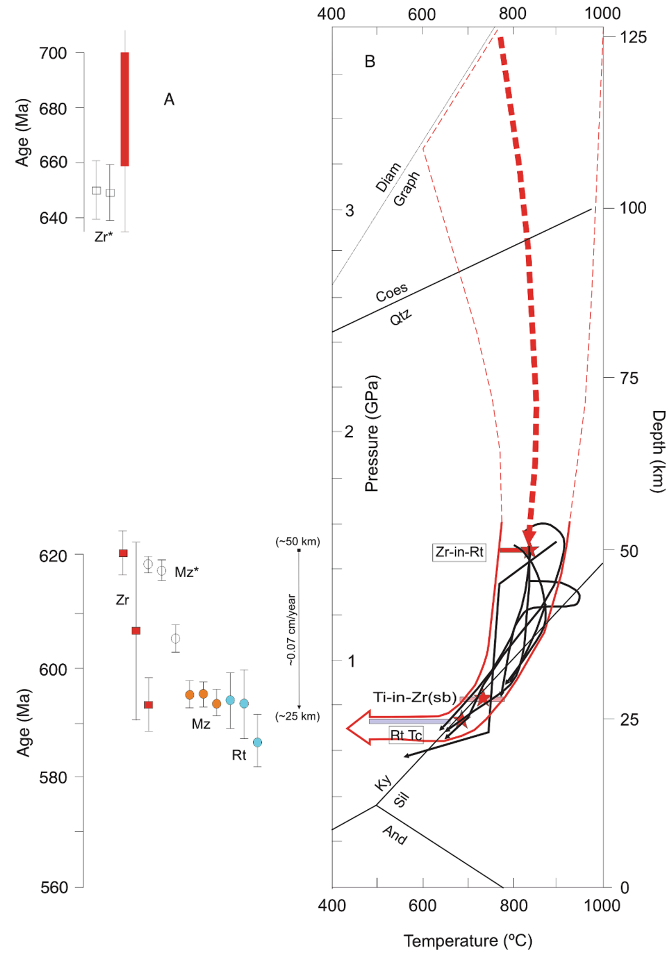

Fig. 10. Pressure–temperature-time (P-T-t) paths interpretation of the (U)HP Três Pontas-Varginha Nappe. (A): U-Pb LA-ICP-MS zircon (Zr), monazite (Mz), and rutile (Rt) ages reported in this work. Previously reported data are open squares (Zr*) U-Pb zircon ages (Reno et al., 2009) and open circles (Mz*) U-Pb ID-TIMS and (U-Th)-Pb EMPA monazite ages (Campos Neto et al., 2010; Motta and Moraes, 2017; Li et al., 2021). Approximative vertical exhumation rates are based on the P-T-t path interpretation; (B): P-T trajectories from Campos Neto and Caby (1999, 2000); Garcia and Campos Neto (2003); Reno et al. (2009); Campos Neto et al. (2010); Motta and Moraes (2017). Colored bars: temperature ranges from Zr-in-Rt, Ti-in Zr thermometers, and the rutile closure temperature (Rt Tc; Kooijman et al., 2010).

observed in metamorphic zircons crystallized under in high-temperature conditions (Rubatto, 2002). Therefore, the 625–620 Myr age obtained from the hand-picked zircon crystals (Fig. 8A) is interpreted as the estimate for the granulite facies metamorphic peak conditions.

Hat-shaped zircon grains around rutile are commonly observed in the analyzed samples (Fig. 4G–H) and are interpreted as a product of Zr exsolution from rutile (Kovaleva et al., 2017) upon decompression and cooling post granulite facies peak metamorphic conditions (e.g., Rubatto, 2017). The 595–585 Myr in-situ U-Pb ages in zircon (Fig. 8B) were mostly obtained from these hat-shaped zircons and are considered as the time-interval of the decompression path under high-temperature conditions (Fig. 10). Ti-in-zircon temperatures (Watson et al., 2006) obtained from hand-picked metamorphic zircons range between 685 and 778 °C (Fig. 9B), similar to the previous reported 700–789 °C Ti-in-biotite temperatures (Li et al., 2021) and are interpreted as temperature record of initial stages of the exhumation path (Fig. 10). Monazite crystals yielded similar ~595 Ma U-Pb in situ ages (Fig. 8D), supporting the exhumation was active around this time interval. These ages were obtained in the gneisses and the analyzed neosome sample (NESG-72Z).

U-Pb in situ ages obtained from the kyanite-bearing gneiss (NESG-93A2) and neosome (NESG-72Z) record monazite crystallization until around 570 Myr (Fig. 8D).

U-Pb in situ ages obtained in rutile grains from both kyanite- and hornblende-bearing gneisses range between 595 Ma and 585 Ma (Fig. 8C). Considering the 640–490 °C core-to-rim closure temperatures for Pb diffusion in rutile (Kooijman et al., 2010) and the common decoupling of Zr-in-rutile temperatures from U-Pb ages in high-grade metamorphism (Ewing et al., 2013), we interpret the in situ ages in rutile as the record of the exhumation path until ~0.7 GPa (Fig. 10).

5.3. Tectonic implications

The ultra-high-pressure metamorphic conditions are recorded by the identification of coesite remnants in quartz inclusions within garnet porphyroblasts (Fig. 7), which are present on the floor (samples NESG-72U) and on the roof (sample NESG-76-6) of the Três Pontas-Varginha Nappe (Fig. 2). Despite the lesser amount of immature quartzites and mafic granulites, the rock package of the Três Pontas-Varginha Nappe is dominated by felsic granulites of pelitic origin (Cioffi et al., 2012; Garcia et al., 2004). The coesite inclusions and the exsolution network of needle-shaped rutile in garnet are first-order evidence to constrain UHP *P-T* paths related to subduction and exhumation of crustal rocks from mantle depths. These data imply that the entire nappe package results from exhumating marine sediments of the distal passive margin from the subduction channel at mantle depths during the onset of the continental collision.

The coesite inclusions in garnet in the felsic rocks described here, along with those included in omphacite in impure marbles in northern Mali (Caby, 1994), are one of the few evidence of Neoproterozoic sedimentary deposits dragged down to mantle depths in the subduction channel and exhumed as a thick and coherent slice of UHP metamorphic rocks. This implies that the leading edge of the São Francisco paleoplate must have been subducted to a minimum coesite-forming depth (90–100 km) beneath the Paranapanema plate (Fig. 11A).

The 625–620 Ma age of the granulite facies metamorphic conditions records the transition from the peak metamorphism to the onset of the exhumation process at ~1.45 Gpa. The 595–585 Myr rutile ages, combined with most of the zircon and monazite ages 595–590 Myr ages, define a time interval of about 25 m.y. for a vertical exhumation from 50

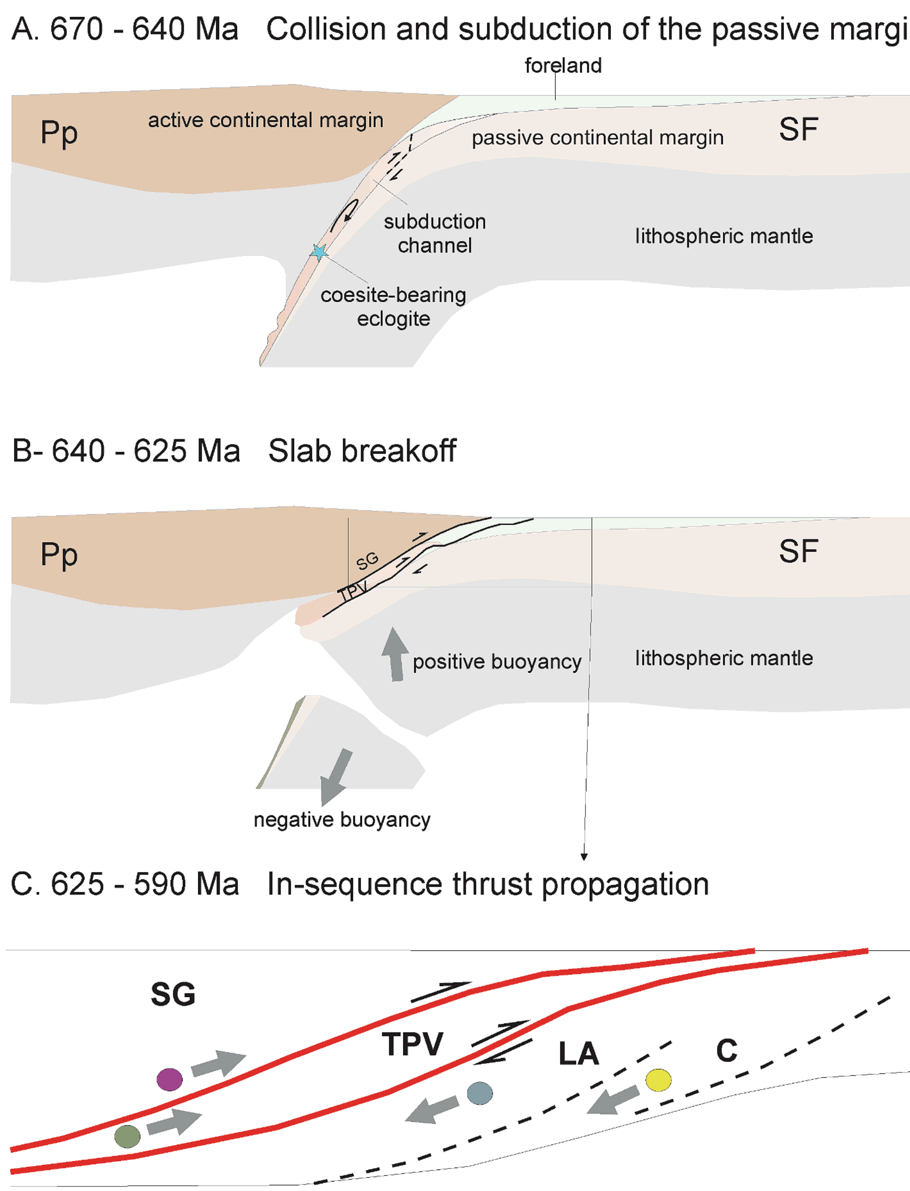

Fig. 11. Tectonic evolution model. Pp-Paranapanema upper plate; SF-São Francisco lower plate; blue star-coesite bearing rocks; SG-Socorro-Guaxupé Nappe; TPV-Três Pontas-Varginha Nappe; LA-Liberdade and Andrelândia nappes; C-Carrancas Nappe System.

km to 25 km depth, resulting in a slow exhumation rate of 0.7 mm/yr.

The identification of microinclusions of coesite associated with the characteristic radial fractures in garnet extends the slices of the UHP terranes of the West Gondwana System of Orogens (Ganade de Araújo et al., 2014) up to the south of the Brasília Orogen (Fig. 1).

5.4. Implications for the São Francisco-Paranapanema collision models

The identification of extensive juvenile Tonian (ca. 800 Ma) mafic-intermediate magmatism related to island arc complexes (Pimentel, 2016; Pimentel et al., 1997; Pimentel and Fuck, 1992 and references therein) marks the initial stages of the subduction-collision evolution of the Brasília Orogen, which evolved to a continental magmatic arc at the northeast margin of the Paranapanema Block (Brito-Neves et al., 1999; Campos Neto, 2000; Matteini et al., 2010; Pimentel et al., 1999; Trouw et al., 2000; Valeriano, 2017; Vinagre et al., 2014). The evidence of a paired metamorphic belt, as a result of these contrasting subduction-collision geodynamic regimes (Campos Neto and Caby, 1999), was highlighted by regional metamorphic apparent thermal gradients across the nappe system of the southernmost edge of the Brasília Orogen (Campos Neto et al., 2020; Marimon et al., 2022; Westin et al., 2021).

The geochronological data reported in the present work is not sufficient to determine the onset of the subduction and collision, requiring consideration of other geological records, especially the estimated age of deposition of flysch deposits in the foreland basin above the passive margin (Fig. 2). The widespread and thick flysch complex trapped in the system of nappes was fed by the erosion of the Tonian island arc terranes and Tonian-Cryogenian continental magmatic rocks during the São Francisco-Paranapanema collision. The sedimentation prograded over the flexed São Francisco basement during the overthrusting of the Paranapanema upper plate and orogenic wedge growth (Fig. 11A). The Cryogenian maximum depositional age ranges between 680 Myr and 640 Myr (Belém et al., 2011; Falci et al., 2018; Frugis et al., 2018; Manoel et al., 2022; Santos, 2011; Rocha et al., 2024; Trouw, 2008; Westin and Campos Neto, 2013). This time interval aligns with previously reported 680–670 Myr ages obtained from retroeclogites of the underneath Liberdade Nappe (Fig. 2) and the 660–650 Myr ages for granulites of the Três Pontas-Varginha Nappe (Campos Neto et al., 2011; Reno et al., 2012, 2009). Hence, we consider that the initial stage of the collision between the São Francisco and Paranapanema paleoplates may have occurred at 680–670 Ma, followed by the subduction of the São Francisco continental crust to mantle depths (>90 km) in the coesite stability field. The Cryogenian 650 Myr ages might record the post-baric UHP metamorphic peak, registered in the analyzed rocks by the decompression textures (i.e., radial fractures and rutile needle-shaped network), which configures the oldest record of coesite micro inclusions in garnets on Earth. Our interpretation implies a protracted convergent process and diachronic closure of the Goiás-Pahrusian Ocean during the building of the West Gondwana Orogen. The sequential collisions along the belt lasted up to 610 Ma at the eastern margin of the West African Craton (Ganade et al., 2023; Ganade de Araújo et al., 2014).

The size of the UHP rock terrane exposed is correlated with the metamorphic duration in the coesite stability field. More extensive UHP expositions experienced protracted UHP metamorphism with slow rates of exhumation, whereas the small ones are related to juvenile crustal protoliths under short timescales of UHP residence and fast rates of exhumation (Kylander-Clark et al., 2012; Zheng, 2012, 2009; Zheng et al., 2019). The presence of garnet porphyroblasts with radial fractures around quartz inclusions, some of them with remaining traces of microcoesite, along with the oriented rutile exsolution lamellae, evidence the UHP metamorphism throughout the nappe pile, suggesting the long duration of the sedimentary protolith within the subduction channel.

The high-pressure granulites of the Três Pontas-Varginha Nappe emerge below the ultra-high temperature Socorro-Guaxupé Nappe, conforming flat-lying and coeval (630–620 Ma) nappe stacks transported for more than 200 km eastward (Section 2.1; Fig. 2), under protracted (up to 590 Ma) sub-solidus metamorphic conditions. The UHT attained by the crustal rocks from the root of the active margin (~40 km depth, Motta et al., 2021; Rocha et al., 2017; Tedeschi et al., 2018) was probably related to the asthenospheric mantle upwelling. The subduction of the continental lithosphere during the collision might have caused an extensional regime within the slab due to opposing buoyancy strength between the slab pull of the more profound and dense lithosphere and the shallower light continental lithosphere. These processes might have resulted in slab breakoff, triggering the rise of the mantle and the UHT metamorphic conditions (Fig. 11B).

Although the temperature conditions and the time length at which the rocks of the Três Pontas-Varginha Nappe remained under UHP within the subduction channel are unknown, the interpretation of the slab breakoff suggests that the granulite facies may not have resulted from an isothermal decompression. It could have resulted, instead, from a subsequent heating event. Similar P-T paths have been modeled for coesite-bearing mafic eclogites from Borborema Province (Gomes et al., 2023) in the central part of the Western Gondwana System of Orogens (Fig. 1B). The high-temperature extrusion from the subduction channel enhanced by the slab-breakoff has also been proposed for the coesite-bearing eclogites of Papua New Guinea and the diamond-coesite-bearing eclogites from the Moldanubian Zone (Faryad et al., 2019; Faryad and Cuthbert, 2020). Alternatively, this geodynamic scenario might be related to the thermal anomaly and crustal melting in the orogen interior, producing the *syn*-to late-orogenic (620–600 Ma) I-type, K-rich calc-alkaline plutonic rocks found in the Socorro-Guaxupé Nappe (Janasi et al., 2023). In contrast, Li et al. (2021) proposed two distinct metamorphic loops for the Três Pontas granulite, based on chemical composition variation of multistage garnet crystals. However, the chemical composition profiles of the garnets analyzed in this work, including those with UHP-like textures (Fig. 5), are not in agreement with this metamorphic scenario.

A deep detachment within the subduction channel probably triggered the uplift of the subducted crustal slice that, allied with the slab breakoff hypothesis, could have caused the subducted crust to lose its dense root, enhancing its buoyancy and upward rise. The decrease of the slab pulls shallows the subduction angle. This interpretation, aligned with those of Chemenda et al. (2000) and O'Brien et al. (2001) for the India–Asia collision, may account for the early detachment of a slice from the subduction channel and its early and partial exhumation to a deep orogenic lower crust (Fig. 11B).

The activation of high-T shear zones at the base of the contiguous Socorro Guaxupé and Três Pontas Varginha nappes marks the onset of the exhumation of the internal orogenic domain. Different models have been proposed for the exhumation of hot orogen cores, e.g. wedge extrusion (Grujic et al., 1996; Hodges et al., 1992; Vannay and Grasemann, 2001), channel flow (Beaumont et al., 2001) and channel flow/extrusion model (Godin et al., 2006), wedge insertion (Webb et al., 2007), thrust propagation to the foreland (DeCelles et al., 2001; Robinson et al., 2006, 2003), critical taper wedge (Kohn, 2008), and foreland propagation of ductile followed by brittle deformation (Carosi et al., 2010, and Montomoli et al., 2013). Although an extensive normal-sense shear zone was not identified at the top of the Três Pontas-Varginha Nappe, our interpretation partially aligns with that of Carosi et al. (2018, 2016, 2010) and Montomoli et al. (2013). An in-sequence process of the thrust-sense shear zone towards E-NE (Fig. 2B) was proposed for the southernmost portion of the Brasília Orogen (Benetti et al., 2024; Campos Neto et al., 2011; Marimon et al., 2022; Westin et al., 2021). This process occurred under high-T (above 590–600 °C) in the kyanite stability field, followed by an isothermal decompression to the sillimanite field, in which each allochthon of the nappe pile reached its metamorphic peak when the upper one was decompressed (Fig. 11C).

6. Conclusions

The granulites and migmatites from Três Pontas-Varginha Nappe comprise the upper allochthon of metasedimentary rocks derived from the distal passive continental margin. They contain coesite micro-inclusions, depicted by Raman spectrometry, in rounded quartz polymorphs within garnet. The remnants of coesite were found within garnet porphyroblasts from rutile-titanite-hornblende-garnet-plagioclase gneiss of the base of the nappe and from (sillimanite-biotite)-rutile-kyanite-garnet-K-feldspar gneisse of the top of the nappe. Radial fractures in garnet around rounded quartz inclusions and the 60°-angled network of needle-shaped rutile and quartz are pervasive throughout the nappe pile.

The coesite and needle-shaped rutile inclusions in garnet define ultra-high-pressure metamorphic conditions for these rocks, implying that the sedimentary deposits of the passive margin were subducted to a minimum coesite-forming depth (>90 km) in the mantle. The UHP metamorphic conditions are also recorded by the chemical composition of garnet porphyroblasts of both felsic (metasedimentary origin) and mafic composition.

Zircon metamorphic overgrowth and soccer-ball crystals record granulite facies metamorphic conditions around 625–620 Ma. In situ ages obtained from zircon, monazite, and rutile crystals record the exhumation path between 595 and 585 Ma. These data reveal a long duration of high-temperature conditions during the decompression.

The continental collision between São Francisco and Paranapanema paleo plates occurred in the Cryogenian, although no robust petrochronological data exists to confirm this hypothesis. Previous works set the maximum depositional age of the flysch deposits over the distal passive margin at 680–640 Ma, constrained the Cryogenian time-lapse for the onset of collision and continental subduction.

CRediT authorship contribution statement

Mario da Costa Campos Neto: Writing – original draft, Visualization, Supervision, Methodology, Investigation, Funding acquisition, Formal analysis, Conceptualization. **Gabriella Labate Frugis:** Writing – original draft, Validation, Methodology, Investigation, Formal analysis, Conceptualization. **Alice Westin:** Writing – review & editing, Validation, Methodology, Investigation, Formal analysis, Conceptualization. **Renaud Caby:** Writing – review & editing, Validation, Conceptualization. **Augusto G. Nobre:** . **Olivier Brugier:** Validation, Investigation, Formal analysis. **Rômulo A. Ando:** .

Declaration of competing interest

The authors declare that they have no known competing financial interests or personal relationships that could have appeared to influence the work reported in this paper.

Data availability

I have shared the data as supplementary material files at the Attach Files step.

Acknowledgments

This research was supported by the São Paulo Research Foundation (FAPESP) through grants 2015/03737-0, 2016/06952-1 (FAPESP/CAPES) and 2017/18174-6. M. C. Campos Neto is a fellow of the Brazilian Research Council (CNPq). The authors also acknowledge the NAP-Geoanalítica core facility of the IGc-USP.

Appendix A. Supplementary material

Supplementary data to this article can be found online at https://doi.org/10.1016/j.precamres.2024.107469.

References

Ague, J.J., Eckert, J.O., 2012. Precipitation of rutile and ilmenite needles in garnet: implications for extreme metamorphic conditions in the Acadian Orogen, U.S.A. Am. Mineral. 97, 840–855. https://doi.org/10.2138/am.2012.4015.

Alifirova, T.A., Pokhilenko, L.N., Ovchinnikov, Y.I., Donnelly, C.L., Riches, A.J.V., Taylor, L.A., 2012. Petrologic origin of exsolution textures in mantle minerals: evidence in pyroxenitic xenoliths from Yakutia kimberlites. Int. Geol. Rev. 54, 1071–1092. https://doi.org/10.1080/00206814.2011.623011.

Alifirova, T.A., Pokhilenko, L.N., Korsakov, A.V., 2015. Apatite, SiO2, rutile and orthopyroxene precipitates in minerals of eclogite xenoliths from Yakutian kimberlites, Russia. Lithos 226, 31–49. https://doi.org/10.1016/j.lithos.2015.01.020.

Amaral, W.S., Santos, F.H., Bravo, J.C.S., Fedel, H.S., Luvizotto, G.L., Godoy, D.F., 2019. U-Pb zircon ages and metamorphic conditions of mafic granulites from the basement of the southern Brasilia Orogen, Campinas-SP region. J. S. Am. Earth Sci. 92, 184–196. https://doi.org/10.1016/j.jsames.2019.02.014.

Axler, J.A., Ague, J.J., 2015. Exsolution of rutile or apatite precipitates surrounding ruptured inclusions in garnet from UHT and UHP rocks. J. Metam. Geol. 33, 829–848. https://doi.org/10.1111/jmg.12145.

Baldwin, S.L., Monteleone, B.D., Webb, L.E., Fitzgerald, P.G., Grove, M., June Hill, E., 2004. Pliocene eclogite exhumation at plate tectonic rates in eastern Papua New Guinea. Nature 431, 263–267. https://doi.org/10.1038/nature02846.

Balis, M., da Campos Neto, M.C., Alves, A., 2020. Serra do Barro Branco orthogneiss: an untimely record of West Gondwana amalgamation in the São Roque Domain. Precambr. Res. 350, 105913 https://doi.org/10.1016/j.precamres.2020.105913.

Basei, M.A.S., Siga Júnior, O., Sato, K., 1995. A metodologia urânio-chumbo na Universidade de São Paulo: Princípios metodológicos, aplicações e resultados obtidos. An. Acad. Bras. Cienc.

Beaumont, C., Jamieson, R.A., Nguyen, M.H., Lee, B., 2001. Himalayan tectonics explained by extrusion of a low-viscosity crustal channel coupled to focused surface denudation. Nature 414, 738–742.

Belém, J., Pedrosa-soares, A.C., Noce, C.M., Carlos, L., Armstrong, R., Fleck, A., Gradim, C., Queiroga, G., 2011. Bacia precursora versus bacias orogênicas: exemplos do Grupo Andrelândia com base em datações U-Pb (LA-ICP-MS) em zircão e análises litoquímicas. Geonomos 19, 224–243.

Benetti, B.Y., 2022. Kinematics and P-T-t Evolution in Hot Collisional Frameworks - Comparison between a Neoproterozoic and Phanerozoic Large Hot Orogens. University of Turin and University of São Paulo, p. 181. Doctoral Thesis.

Benetti, B., da Campos Neto, M.C., Carosi, R., Luvizotto, G., Iaccarino, S., Montomoli, C., 2024. In-sequence tectonic evolution of Ediacaran nappes in the southeastern branch of the Brasília Orogen (SE Brazil): constraints from metamorphic iterative thermodynamic modeling and monazite petrochronology. Lithos 464–465, 107459. https://doi.org/10.1016/j.lithos.2023.107459.

Bosch, D., Garrido, C.J., Bruguier, O., Dhuime, B., Bodinier, J.-L., Padròn-Navarta, J.A., Galland, B., 2011. Building an island-arc crustal section: time constraints from a LA-ICP-MS zircon study. Earth Planet. Sci. Lett. 309, 268–279. https://doi.org/10.1016/j.epsl.2011.07.016.

Brito-Neves, B.B., Campos Neto, M.C., Fuck, R.A., 1999. From Rodinia to Western Gondwana: an approach to the Brasiliano-Pan African Cycle and orogenic collage. Episodes 22, 155–166.

Brown, M., Johnson, T., 2018. Secular change in metamorphism and the onset of global plate tectonics. Am. Mineral. 103, 181–196. https://doi.org/10.2138/am-2018-6166.

Bruguier, O., Bosch, D., Caby, R., Vitale-Brovarone, A., Fernandez, L., Hammor, D., Laouar, R., Ouabadi, A., Abdallah, N., Mechati, M., 2017. Age of UHP metamorphism in the Western Mediterranean: insight from rutile and minute zircon inclusions in a diamond-bearing garnet megacryst (Edough Massif, NE Algeria). Earth Planet. Sci. Lett. 474, 215–225. https://doi.org/10.1016/j.epsl.2017.06.043.

Bucher, K., Frey, M., 2002. Petrogenesis of Metamorphic Rocks. Springer-Verlag, Berlin Heidelberg.

Caby, R., 1994. Precambrian coesite from northern Mali: first record and implications for plate tectonics in the trans-Saharan segment of the Pan-African belt. Eur. J. Mineral. 6, 235–244. https://doi.org/10.1127/ejm/6/2/0235.

Caby, R., 2003. Terrane assembly and geodynamic evolution of central–western Hoggar: a synthesis. J. African Earth Sci. 37, 133–159. https://doi.org/10.1016/j.jafrearsci.2003.05.003.

Caby, R., Bruguier, O., Fernandez, L., Hammor, D., Bosch, D., Mechati, M., Laouar, R., Ouabadi, A., Abdallah, N., Douchet, C., 2014. Metamorphic diamonds in a garnet megacryst from the Edough Massif (northeastern Algeria). Recognition and geodynamic consequences. Tectonophysics 637, 341–353. https://doi.org/10.1016/j.tecto.2014.10.017.

Campos Neto, M.C., Basei, M.A.S., Janasi, V.A., Moraes, R., 2011. Orogen migration and tectonic setting of the Andrelândia Nappe system: an Ediacaran western Gondwana collage, south of São Francisco craton. J. S. Am. Earth Sci. 32, 393–406.

Campos Neto, M.C., Caby, R., 1999. Neoproterozoic high-pressure metamorphism and tectonic constraint from the nappe system south of the Sao Francisco Craton, southeast Brazil. Precambr. Res. 97, 3–26.

Campos Neto, M.C., Caby, R., 2000. Lower crust extrusion and terrane accretion in the Neoproterozoic nappes of southeast Brazil. Tectonics 19, 669–687.

Campos Neto, M.C., Cioffi, C.R., Westin, A., Rocha, B.C., Frugis, G.L., Tedeschi, M., Pinheiro, M.A.P., 2020. O Orógeno Brasília Meridional. In: Bartorelli, A., Teixeira, W., Brito-Neves, B.B. (Eds.), Geocronologia e Evolução Tectônica Do Continente Sul-

Americano: A Contribuição de Umberto Giuseppe Cordani. Solaris Edições Culturais, pp. 146–180.
Campos Neto, M.C., Janasi, V.A., Basei, M.A.S., Siga Jr., O., 2007. Sistema de nappes Andrelândia, setor oriental: litoestratigrafia e posição estratigráfica. Rev. Bras. Geociências 37, 47–60.
Campos Neto, M.C., Cioffi, C.R., Moraes, R., Motta, R.G., Siga Jr., O., Basei, M.A.S., 2010. Structural and metamorphic control on the exhumation of high-P granulites: the Carvalhos Klippe example, from the oriental Andrelândia Nappe System, southern portion of the Brasília Orogen, Brazil. Precambr. Res. 180, 125–142. https://doi.org/10.1016/j.precamres.2010.05.010.
Campos Neto, M.C., 2000. Orogenic systems from southwestern Gondwana: an approach to Brasiliano-Pan African Cycle and orogenic collage in Southeastern Brazil. In: Cordani, U.G., Milani, E.J., Thomaz Filho, A., Campos, D.A. (Eds.), Tectonic Evolution of South America. Rio de Janeiro, pp. 335–365.
Carosi, R., Montomoli, C., Rubatto, D., Visonà, D., 2010. Late Oligocene high-temperature shear zones in the core of the Higher Himalayan Crystallines (Lower Dolpo, western Nepal). Tectonics 29. https://doi.org/10.1029/2008TC002400.
Carosi, R., Montomoli, C., Iaccarino, S., Massonne, H.-J., Rubatto, D., Langone, A., Gemignani, L., Visonà, D., 2016. Middle to late Eocene exhumation of the Greater Himalayan Sequence in the Central Himalayas: progressive accretion from the Indian plate. Bull. Geol. Soc. Am. 128, 1571–1592. https://doi.org/10.1130/B31471.1.
Carosi, R., Montomoli, C., Iaccarino, S., 2018. 20 years of geological mapping of the metamorphic core across Central and Eastern Himalayas. Earth-Sci. Rev. 177, 124–138. https://doi.org/10.1016/j.earscirev.2017.11.006.
Carvalho, B.R.B.M., Trouw, R.A.J., Cintra da Costa, R.V., Ribeiro, A., Heilbron, M., Marimon, R.S., 2020. Microstructural and metamorphic evolution of the Carrancas Klippe, interference zone of the Neoproterozoic southern Brasilia and Ribeira orogens, SE Brazil. J. S. Am. Earth Sci., 102744 https://doi.org/10.1016/j.jsames.2020.102744.
Caxito, F.A., Hartmann, L.A., Heilbron, M., Pedrosa-Soares, A.C., Bruno, H., Basei, M.A.S., Chemale, F., 2022. Multi-proxy evidence for subduction of the Neoproterozoic Adamastor Ocean and Wilson cycle tectonics in the South Atlantic Brasiliano Orogenic System of Western Gondwana. Precambr. Res. 376 https://doi.org/10.1016/j.precamres.2022.106678.
Chemenda, A.I., Mattauer, M., Malavieille, J., Bokun, A.N., 1995. A mechanism for syn-collisional rock exhumation and associated normal faulting: results from physical modelling. Earth Planet. Sci. Lett. 132, 225–232.
Chemenda, A.I., Burg, J.P., Mattauer, M., 2000. Evolutionary model of the Himalaya-Tibet system: geopoem based on new modelling, geological and geophysical data. Earth Planet. Sci. Lett. 174, 397–409. https://doi.org/10.1016/S0012-821X(99)00277-0.
Chopin, C., 1984. Coesite and pure pyrope in high-grade blueschists of the Western Alps: a first record and some consequences. Contrib. Mineral. Petrol. 86, 107–118. https://doi.org/10.1007/BF00381838.
Chopin, C., 2003. Ultrahigh-pressure metamorphism: tracing continental crust into the mantle. Earth Planet. Sci. Lett. 212, 1–14. https://doi.org/10.1016/S0012-821X(03)00261-9.
Cioffi, C.R., da Campos Neto, M.C., da Rocha, B.C., Moraes, R., Henrique-Pinto, R., 2012. Geochemical signatures of metasedimentary rocks of high-pressure granulite facies and their relation with partial melting: Carvalhos Klippe, Southern Brasília Belt, Brazil. J. South Am. Earth Sci. 40, 63–76. https://doi.org/10.1016/j.jsames.2012.09.007.
Cioffi, C.R., da Campos Neto, M.C., Möller, A., Rocha, B.C., 2016a. Tectonic significance of the Meso- to Neoarchean complexes in the basement of the southern Brasília Orogen. Precambr. Res. 287, 91–107. https://doi.org/10.1016/j.precamres.2016.10.009.
Cioffi, C.R., Campos Neto, M.C., Möller, A., Rocha, B.C., 2016b. Paleoproterozoic continental crust generation events at 2.15 and 2.08 Ga in the basement of the southern Brasília Orogen, SE Brazil. Precambr. Res. 275, 176–196. https://doi.org/10.1016/j.precamres.2016.01.007.
Coelho, M.B., Trouw, R.A.J., Ganade, C.E., Vinagre, R., Mendes, J.C., Sato, K., 2017. Constraining timing and P-T conditions of continental collision and late overprinting in the Southern Brasília Orogen (SE-Brazil): U-Pb zircon ages and geothermobarometry of the Andrelândia Nappe System. Precambr. Res. 292, 194–215. https://doi.org/10.1016/j.precamres.2017.02.001.
Costa, F.M., Penna, J.L.A., Martins, L.C.D., Tedeschi, M., Novo, T.A., Araujo, C.S., Rossi, P.L.V., Lana, C., Pedrosa-Soares, A.C., 2022. Zircon petrochronology reveals the moderately juvenile signature of a diatexite from the boundary zone between the Brasília and Ribeira orogens (SE Brazil): relict of a Tonian arc? J. S. Am. Earth Sci. 116 https://doi.org/10.1016/j.jsames.2022.103767.
Costa, R.V., Trouw, R.A.J., Mendes, J.C., 2018. Geologia e geocronologia do charnockito São Francisco Xavier e do gabronorito Ribeirão do Paiol (MG/SP) e suas póssíveis relações com processos curstais extensionais nos orógenos Brasília Meridional e Ribeira Central. Geol. USP - Ser. Cient. 18, 85–102. https://doi.org/10.11606/ISSN.2316-9095.V18-401.
de Janasi, V.A., Martins, L., Alves, A., Simonetti, A., Henrique-Pinto, R., 2023. The Neoproterozoic Agudos Grandes granitic batholith, SE Brazil: inferences on source areas from elemental and Sr-Nd-Pb isotope geochemistry. J. S. Am. Earth Sci. 130, 104570 https://doi.org/10.1016/j.jsames.2023.104570.
DeCelles, P.G., Robinson, D.M., Quade, J., Ojha, T.P., Garzione, C.N., Copeland, P., Upreti, B.N., 2001. Stratigraphy, structure, and tectonic evolution of the Himalayan fold-thrust belt in western Nepal. Tectonics 20, 487–509.
Del Lama, E.A., Zanardo, A., Oliveira, M.A.F., Morales, N., 2000. Exhumation of high-pressure granulites of the Guaxupé complex, Southeastern Brazil. Geol. J. 35, 231–249.
Dobrzhinetskaya, L.F., Faryad, S.W., 2011. Frontiers of ultrahigh-pressure metamorphism: view from field and laboratory. In: Dobrzhinetskaya, L. F., Faryad, S. W., Wallis, S., Cuthbert, S.J. (Eds.), Ultrahigh-Pressure Metamorphism: 25 Years After The Discovery Of Coesite and Diamond. Elsevier, pp. 1–39. doi: 10.1016/B978-0-12-385144-4.00020-5.
Duffles, P.A., Trouw, R.A.J., Mendes, J.C., Gerdes, A., 2013. Marins Granite (MG/SP): petrography, geochemistry, geochronology, and geotectonic setting. Braz. J. Geol. 43, 487–500. https://doi.org/10.5327/Z2317-48892013000300006.
Ebert, H.D., Chemale Jr., F., Babinski, M., Artur, A.C., Van Schmus, W.R., 1996. Tectonic setting and U-Pb zircon dating of the plutonic Socorro Complex in the transpressive Rio Paraíba do Sul shear belt, SE Brazil. Tectonics 15, 688–699.
Ewing, T.A., Hermann, J., Rubatto, D., 2013. The robustness of the Zr-in-rutile and Ti-in-zircon thermometers during high-temperature metamorphism (Ivrea-Verbano Zone, northern Italy). Contrib. Mineral. Petrol. 165, 757–779. https://doi.org/10.1007/s00410-012-0834-5.
Falci, A., de Andrade Caxito, F., Seer, H.J., de Morisson Valeriano, C., Dias, P.H.A., Pedrosa-Soares, A.C., 2018. Provenance shift from a continental margin to a syn-orogenic basin in the Neoproterozoic Araxá nappe system, southern Brasília belt, Brazil. Precambr. Res. 306, 209–219. https://doi.org/10.1016/j.precamres.2018.01.004.
Faryad, S.W., Baldwin, S.L., Jedlicka, R., Ježek, J., 2019. Two-stage garnet growth in coesite eclogite from the southeastern Papua New Guinea (U)HP terrane and its geodynamic significance. Contrib. Mineral. Petrol. 174, 73 https://doi.org/10.1007/s00410-019-1612-4.
Faryad, S.W., Cuthbert, S.J., 2020. High-temperature overprint in (U)HPM rocks exhumed from subduction zones; a product of isothermal decompression or a consequence of slab break-off (slab rollback)? Earth-Sci. Rev. 202, 103108 https://doi.org/10.1016/j.earscirev.2020.103108.
Fontainha, M.V.F., Trouw, R.A.J., Dantas, E.L., Polo, H.J.O., Furtado, P.C., Marimon, R.S., Telles, R.C.M., Peternel, R., 2021. Provenance and tectonic evolution of the Andrelândia Group in the region between the Socorro and Guaxupé nappes, Southern Brasília and Ribeira orogens, Brazil. J. South Am. Earth Sci. 109, 103060 https://doi.org/10.1016/j.jsames.2020.103060.
Frank, O., Zukalova, M., Laskova, B., Kürti, J., Koltai, J., Kavan, L., 2012. Raman spectra of titanium dioxide (anatase, rutile) with identified oxygen isotopes (16, 17, 18). PCCP 14, 14567–14572. https://doi.org/10.1039/C2CP42763J.
Frugis, G.L., Campos Neto, M.C., Lima, R.B., 2018. Eastern Paranapanema and southern São Francisco orogenic margins: records of enduring Neoproterozoic oceanic convergence and collision in the southern Brasília Orogen. Precambr. Res. 308, 35–57. https://doi.org/10.1016/j.precamres.2018.02.005.
Fuck, R.A., Pimentel, M.M., Alvarenga, C.J.S., Dantas, E.L., 2017. The Northern Brasília Belt BT - São Francisco Craton, Eastern Brazil: Tectonic Genealogy of a Miniature Continent. In: Heilbron, M., Cordani, U.G., Alkmim, F.F. (Eds.), Springer International Publishing, Cham, pp. 205–220. doi: 10.1007/978-3-319-01715-0_11.
Fumes, R.A., Luvizotto, G.L., Moraes, R., Heilbron, M., Vlach, S.R.F., 2019. Metamorphic modeling and petrochronology of metapelitic rocks from the Luminárias Nappe, southern Brasília belt (SE Brazil). Braz. J. Geol. 49 https://doi.org/10.1590/2317-4889201920180114.
Fumes, R.A., Luvizotto, G.L., Moraes, R., Patto, L.A., 2021. The potential for using metagreywacke to study metamorphism of amphibolite facies conditions: a comparison study within the Luminárias Nappe, Southern Brasília Orogen (Southeastern Brazil). Mineral. Petrol. 115, 519–534. https://doi.org/10.1007/s00710-021-00758-8.
Ganade de Araújo, C.E., Rubatto, D., Hermann, J., Cordani, U.G., Caby, R., Basei, M.A.S., 2014. Ediacaran 2,500-km-long synchronous deep continental subduction in the West Gondwana Orogen. Nat. Commun. 5, 5198 https://doi.org/10.1038/ncomms6198.
Ganade, C.E., Rubatto, D., Lanari, P., Hermann, J., Tesser, L.R., Caby, R., 2023. Fast exhumation of Earth's earliest ultrahigh-pressure rocks in the West Gondwana orogen, Mali. Geology 51, 647–651. https://doi.org/10.1130/G50998.1.
Garcia, M.G.M., Campos Neto, M.C., 2003. Contrasting metamorphic conditions in the Neoproterozoic collision-related Nappes south of São Francisco Craton, SE Brazil. J. S. Am. Earth Sci. 15, 853–870.
Garcia, M.G.M., Campos Neto, M.C., Janasi, V.A., 2004. Proveniência e ambientação tectônica de metassedimentos de alto grau: Nappe Três Pontas-Varginha, sul do Cráton São Francisco. Rev. Bras. Geociências 34, 49–58. https://doi.org/10.25249/0375-7536.20043414958.
Gengo, R.M., 2014. Petrologia de ortognaisses e granitóides do domínio Socorro, Nappe Socorro-Guaxupé, seção Extrema-Camanducaia. Unpublished Master's Dissertation - Instituto de Geociências, Universidade de São Paulo.
Gillet, P., Ingrin, J., Chopin, C., 1984. Coesite in subducted continental crust: P-T history deduced from an elastic model. Earth Planet. Sci. Lett. 70, 426–436. https://doi.org/10.1016/0012-821X(84)90026-8.
Godin, L., Grujic, D., Law, R.D., Searle, M.P., 2006. Channel flow, ductile extrusion and exhumation in continental collision zones: an introduction. Geol. Soc. Spec. Publ. 268, 1–23. https://doi.org/10.1144/GSL.SP.2006.268.01.01.
Gomes, N.B., dos Santos, T.J.S., Tedeschi, M., Galante, D., Luvizotto, G.L., 2023. P-T-t reconstruction of a coesite-bearing retroeclogite reveals a new UHP occurrence in the Western Gondwana margin (NE-Brazil). Lithos 446–447. https://doi.org/10.1016/j.lithos.2023.107138.
Griffin, W.L., Jensen, B.B., Misra, S.N., 1971. Anomalously elongated rutile in eclogite-facies pyroxene and garnet. Nor. Geol. Tidsskr. 51, 177–185.
Grujic, D., Casey, M., Davidson, C., Hollister, L.S., Kündig, R., Pavlis, T., Schmid, S., 1996. Ductile extrusion of the Higher Himalayan Crystalline in Bhutan: evidence from quartz microfabrics. Tectonophysics 260, 21–43. https://doi.org/10.1016/0040-1951(96)00074-1.

Hemley, R.J., 1987. Pressure Dependence of Raman Spectra of SiO2 Polymorphs: α-Quartz, Coesite, and Stishovite. In: High-Pressure Research in Mineral Physics: A Volume in Honor of Syun-iti Akimoto. American Geophysical Union (AGU), pp. 347–359. doi: 10.1029/GM039p0347.

Hodges, K.V., Parrish, R.R., Housh, T.B., Lux, D.R., Burchfiel, B.C., Royden, L.H., Chen, Z., 1992. Simultaneous miocene extension and shortening in the Himalayan Orogen. Science (80-) 258, 1466–1470. https://doi.org/10.1126/science.258.5087.1466.

Hoskin, P.W.O., Schaltegger, U., 2003. The composition of zircon and igneous and metamorphic petrogenesis. In: Hanchar, J.M., Hoskin, P.W.O. (Eds.), Zircon - Reviews in Mineralogy and Geochemistry. Mineralogical Society of America and Geochemical Society, pp. 27–62.

Hwang, S.L., Yui, T.F., Chu, H.T., Shen, P., Schertl, H.P., Zhang, R.Y., Liou, J.G., 2007. On the origin of oriented rutile needles in garnet from UHP eclogites. J. Metam. Geol. 25, 349–362. https://doi.org/10.1111/j.1525-1314.2007.00699.x.

Jahn, B., Caby, R., Monie, P., 2001. The oldest UHP eclogites of the World: age of UHP metamorphism, nature of protoliths and tectonic implications. Chem. Geol. 178, 143–158. https://doi.org/10.1016/S0009-2541(01)00264-9.

Janasi, V.A., Vlach, S.R.F., Campos Neto, M.C., Ulbrich, H.H.G.J., 2009. Associated A-type subalkaline and high-K calc-alkaline granites in the Itu Granite Province, southeastern Brazil: petrological and tectonic significance. Can. Mineral. 47, 1505–1526. https://doi.org/10.3749/canmin.47.6.1505.

Keller, D.S., Ague, J.J., 2020. Quartz, mica, and amphibole exsolution from majoritic garnet reveals ultra-deep sediment subduction, Appalachian Orogen. Sci. Adv. 6, eaay5178.

Kohn, M.J., 2008. P-T-t data from central Nepal support critical taper and repudiate large-scale channel flow of the Greater Himalayan Sequence. GSA Bull. 120, 259–273. https://doi.org/10.1130/B26252.1.

Kooijman, E., Mezger, K., Berndt, J., Smit, M., 2010. The decoupling of the Zr- and U-Pb systematics in rutile during cooling from HT conditions. In: EGU General Assembly 2010. p. vol 12.

Kovaleva, E., Austrheim, H.O., Klötzli, U.S., 2017. Interpretation of zircon coronae textures from metapelitic granulites of the Ivrea-Verbano Zone, northern Italy: two-stage decomposition of Fe-Ti oxides. Solid Earth 8, 789–804. https://doi.org/10.5194/se-8-789-2017.

Kuster, K., Ribeiro, A., Trouw, R.A.J., Dussin, I., Marimon, R.S., 2020. The Neoproterozoic Andrelândia group: evolution from an intraplate continental margin to an early collisional basin south of the São francisco craton, Brazil. J. South Am. Earth Sci. 102 https://doi.org/10.1016/j.jsames.2020.102666.

Kylander-Clark, A.R.C., Hacker, B.R., Mattinson, C.G., 2012. Size and exhumation rate of ultrahigh-pressure terranes linked to orogenic stage. Earth Planet. Sci. Lett. 321–322, 115–120. https://doi.org/10.1016/j.epsl.2011.12.036.

Lana, C., Farina, F., Gerdes, A., Alkmim, A., Gonçalves, G.O., Jardim, A.C., 2017. Characterization of zircon reference materials via high precision U-Pb LA-MC-ICP-MS. J. Anal. At. Spectrom 32, 2011–2023. https://doi.org/10.1039/C7JA00167C.

Li, B., Massonne, H.-J., Hartmann, L.A., Zhang, J., Luo, T., 2021. Kyanite-garnet granulite from the Andrelândia nappe system, Brasília belt, registers two late Neoproterozoic metamorphic cycles. Precambr. Res. 355, 106086 https://doi.org/10.1016/j.precamres.2020.106086.

Liu, L., Zhang, J., Green, H.W., Jin, Z., Bozhilov, K.N., 2007. Evidence of former stishovite in metamorphosed sediments, implying subduction to >350 km. Earth Planet. Sci. Lett. 263, 180–191. https://doi.org/10.1016/J.EPSL.2007.08.010.

Ludwig, K.R., 2008. User's manual for Isoplot 3.70 - A geochronological toolkit for Microsoft Excel. Berkeley Geochronol. Cent. Spec. Publ. 76.

Manoel, T.N., Heilbron, M., Cutts, K., Dussin, I., Marins, G., Jailane, Lobato, M., de Morisson Valeriano, C., Bruno, H., 2022. An example of a Neoproterozoic hyperextended margin: an integrated perspective of the basic magmatism recorded in the Andrelândia Basin, central Ribeira Orogen, SE-Brazil. Precambr. Res. 381, 106863 https://doi.org/10.1016/j.precamres.2022.106863.

Manzotti, P., Schiavi, F., Nosenzo, F., Pitra, P., Ballèvre, M., 2022. A journey towards the forbidden zone: a new, cold, UHP unit in the Dora-Maira Massif (Western Alps). Contrib. Mineral. Petrol. 177, 59 https://doi.org/10.1007/s00410-022-01923-8.

Marimon, R.S., Trouw, R.A.J., Dantas, E.L., Ribeiro, A., 2020. U-Pb and Lu-Hf isotope systematics on detrital zircon from the southern São Francisco Craton's Neoproterozoic passive margin: tectonic implications. J. S. Am. Earth Sci. 100 https://doi.org/10.1016/j.jsames.2020.102539.

Marimon, R.S., Hawkesworth, C.J., Trouw, R.A.J., Trouw, C., Dantas, L., Ribeiro, A., Vinagre, R., Hackspacher, P., Avila, C., Motta, R., Moraes, R., 2022. Subduction and continental collision in the Neoproterozoic: Sanukitoid-like magmatism and paired metamorphism in SE Brazil. Precambr. Res. 383, 106888 https://doi.org/10.1016/j.precamres.2022.106888.

Marimon, R.S., Trouw, R.A.J., Hawkesworth, C.J., Waterkemper, J., Ribeiro, A., Vinagre, R., Dantas, E.L., 2023. Challenges of dating metasedimentary successions in collisional orogens: a case study of a Neoproterozoic passive margin in West Gondwana. Gondw. Res. 113, 1–13. https://doi.org/10.1016/j.gr.2022.10.002.

Martinez, J.A.E., Sanchez Junior, M., Golçalves, A.N., Orrego, R.M.M., Florêncio, O., 2021. Influence of different oxidation mechanisms on the exfoliation of intercalated graphite bisulfate using two types of graphite. Rev. Mater. 26 https://doi.org/10.1590/S1517-707620210002.1293.

Massonne, H.-J., 2003. A comparison of the evolution of diamondiferous quartz-rich rocks from the Saxonian Erzgebirge and the Kokchetav Massif: are so-called diamondiferous gneisses magmatic rocks? Earth Planet Sci. Lett. 216, 347–364. https://doi.org/10.1016/S0012-821X(03)00512-0.

Massonne, H.-J., Li, B., 2020. Zoning of eclogitic garnet cores – a key pattern demonstrating the dominance of tectonic erosion as part of the burial process of worldwide occurring eclogites. Earth-Sci. Rev. 210, 103356 https://doi.org/10.1016/j.earscirev.2020.103356.

Matteini, M., Junges, S.L., Dantas, E.L., Pimentel, M.M., Bühn, B., 2010. In situ zircon U-Pb and Lu–Hf isotope systematic on magmatic rocks: insights on the crustal evolution of the Neoproterozoic Goiás Magmatic Arc, Brasília belt, Central Brazil. Gondwana Res. 17, 1–12. https://doi.org/10.1016/j.gr.2009.05.008.

Mazza, T., Barborini, E., Piseri, P., Milani, P., Cattaneo, D., Li Bassi, A., Bottani, C.E., Ducati, C., 2007. Raman spectroscopy characterization of Ti O2 rutile nanocrystals. Phys. Rev. B - Condens. Matter Mater. Phys. 75, 1–5. https://doi.org/10.1103/PhysRevB.75.045416.

Montomoli, C., Iaccarino, S., Carosi, R., Langone, A., Visonà, D., 2013. Tectonometamorphic discontinuities within the Greater Himalayan Sequence in Western Nepal (Central Himalaya): insights on the exhumation of crystalline rocks. Tectonophysics 608, 1349–1370. https://doi.org/10.1016/j.tecto.2013.06.006.

Mora, C.A.S., Campos Neto, M.C., Basei, M.A.S., 2014. Syn-collisional lower continental crust anatexis in the Neoproterozoic Socorro-Guaxupé Nappe System, southern Brasília Orogen, Brazil: constraints from zircon U-Pb dating, Sr–Nd–Hf signatures and whole-rock geochemistry. Precambr. Res. 255, 847–864.

Motta, R.G., Fitzsimons, I.C.W., Moraes, R., Johnson, T.E., Schuindt, S., Benetti, B.Y., 2021. Recovering P-T–t paths from ultra-high temperature (UHT) felsic orthogneiss: an example from the Southern Brasília Orogen, Brazil. Precambr. Res. 359, 106222 https://doi.org/10.1016/j.precamres.2021.106222.

Motta, R.G., Moraes, R., 2017. Pseudo- and real-inverted metamorphism caused by the superposition and extrusion of a stack of nappes: a case study of the Southern Brasília Orogen, Brazil. Int. J. Earth Sci. (Geol. Rundsch) 106, 2407–2427. https://doi.org/10.1007/s00531-016-1436-7.

Mposkos, E.D., Kostopoulos, D.K., 2001. Diamond, former coesite and supersilicic garnet in metasedimentary rocks from the Greek Rhodope: a new ultrahigh-pressure metamorphic province established. Earth Planet. Sci. Lett. 192, 497–506. https://doi.org/10.1016/S0012-821X(01)00478-2.

Nobre, A.G., Martínez, J.A.E., Terence, M.C., Florêncio, O., 2020. The action of shear zones in the natural availability of graphite nanoplatelets: the example of the metadolomites of the Itaiacoca Group and the mica schist of the Dom Silverio Group. Braz. J. Anim. Environ. Res. 3, 3108–3118. https://doi.org/10.34188/bjaerv3n4-031.

Nobre, A.G., Salazar-Naranjo, A.F., de Andrade, F.R.D., Vlach, S.R.F., Ando, R.A., 2022. Simulation of geological graphene genesis by the piston-cylinder apparatus. Rev. Mater. 27 https://doi.org/10.1590/1517-7076-rmat-2022-0122.

O'Brien, P.J., Zotov, N., Law, R., Khan, M.A., Jan, M.Q., 2001. Coesite in Himalayan eclogite and implications for models of India-Asia collision. Geology 29, 435. https://doi.org/10.1130/0091-7613(2001)029<0435:CIHEAI>2.0.CO;2.

Oliveira, M.A.F., de Negri, F.A., Zanardo, A., 2019. Archean and paleoproterozoic crust generation events, Amparo complex and Serra Negra orthogneiss in southern Brasília Orogen, SE Brazil. J. S. Am. Earth Sci. 90, 137–154. https://doi.org/10.1016/j.jsames.2018.11.029.

Parkinson, C., 2000. Coesite inclusions and prograde compositional zonation of garnet in whiteschist of the HP-UHPM Kokchetav massif, Kazakhstan: a record of progressive UHP metamorphism. Lithos 52, 215–233. https://doi.org/10.1016/S0024-4937(99)00092-4.

Parkinson, C.D., Katayama, I., 1999. Present-day ultrahigh-pressure conditions of coesite inclusions in zircon and garnet: evidence from laser Raman microspectroscopy. Geology 27, 979–982. https://doi.org/10.1130/0091-7613(1999)027<0979:PDUPCO>2.3.CO;2.

Parkinson, C.D., Motoki, A., Onishi, C.T., Maruyama, S., 2001. Ultrahigh-pressure pyrope-kyanite granulites and associated eclogites in Neoproterozoic nappes of southeast Brazil. In: UHPM Workshop. Waseda, Tokyo, pp. 87–90.

Peternel, R., Trouw, R.A.J., da Schmitt, R.S., 2005. Interferência entre duas faixas móveis Neoproterozóicas: o caso das faixas Brasília e Ribeira no sudeste do Brasil. Rev. Bras. Geociências 35, 297–310.

Pimentel, M.M., 2016. The tectonic evolution of the Neoproterozoic Brasília Belt, central Brazil: a geochronological and isotopic approach. Braz. J. Geol. 46, 67–82. https://doi.org/10.1590/2317-4889201620150004.

Pimentel, M.M., Fuck, R.A., 1992. Neoproterozoic crustal accretion in central Brazil. Geology 20, 375–379.

Pimentel, M.M., Whitehouse, M.J., Viana, M.G., Fuck, R.A., Nuno, M., 1997. The Mara Rosa Arch in the Tocantins Province: further evidence for Neoproterozoic crustal accretion in Central Brazil. Precambr. Res. 81, 299–310. https://doi.org/10.1016/S0301-9268(96)00039-3.

Pimentel, M.M., Fuck, R.A., Botelho, N.F., 1999. Granites and the geodynamic history of the neoproterozoic Brasília belt, Central Brazil: a review. Lithos 46, 463–483. https://doi.org/10.1016/S0024-4937(98)00078-4.

Pinheiro, M.A.P., Suita, M.T.F., Lesnov, F.P., Tedeschi, M., Silva, L.C., Medvedev, N.S., Korolyuk, V.N., Pinto, C.P., Sergeev, S.A., 2019. Timing and petrogenesis of metamafic-ultramafic rocks in the Southern Brasília orogen: insights for a Rhyacian multi-system suprasubduction zone in the São Francisco paleocontinent (SE-Brazil). Precambr. Res. 321, 328–348. https://doi.org/10.1016/j.precamres.2018.12.006.

Quéméneur, J.J.G., Ribeiro, A., Paciullo, F.V.P., Heilbron, M., Trouw, R.A.J., Valença, J.G., Noce, C.M., 2003. Mapa Geológico - Folha Lavras.

Reno, B.L., Brown, M., Kobayashi, K., Nakamura, E., Piccoli, P.M., Trouw, R.A.J., 2009. Eclogite-high-pressure granulite metamorphism records early collision in West Gondwana: new data from the Southern Brasilia Belt, Brazil. J. Geol. Soc. London. 166, 1013–1032. https://doi.org/10.1144/0016-76492008-140.

Reno, B.L., Piccoli, P.M., Brown, M., Trouw, R.A.J., 2012. In situ monazite (U-Th)-Pb ages from the Southern Brasilia Belt, Brazil: constraints on the high-temperature retrograde evolution of HP granulites. J. Metam. Geol. 30, 81–112. https://doi.org/10.1111/j.1525-1314.2011.00957.x.

Ribeiro, A., Heilbron, M., 1982. Estratigrafia e metamorfismo dos Grupos Carrancas e Andrelândia, sul de Minas Gerais. In: XXXII Congresso Brasileiro De Geologia. Salvador, pp. 177–186.

Robinson, D.M., DeCelles, P.G., Garzione, C.N., Pearson, O.N., Harrison, T.M., Catlos, E.J., 2003. Kinematic model for the Main Central thrust in Nepal. Geology 31, 359–362. https://doi.org/10.1130/0091-7613-31.1.e41.

Robinson, D.M., DeCelles, P.G., Copeland, P., 2006. Tectonic evolution of the Himalayan thrust belt in western Nepal: implications for channel flow models. GSA Bull. 118, 865–885. https://doi.org/10.1130/B25911.1.

Rocha, B.C., Moraes, R., Möller, A., Cioffi, C.R., Jercinovic, M.J., 2017. Timing of anatexis and melt crystallization in the Socorro-Guaxupé Nappe, SE Brazil: insights from trace element composition of zircon, monazite and garnet coupled to U—Pb geochronology. Lithos 277, 337–355. https://doi.org/10.1016/j.lithos.2016.05.020.

Rocha, B.C., Moraes, R., Möller, A., Cioffi, C.R., 2018. Magmatic inheritance vs. UHT metamorphism: zircon petrochronology of granulites and petrogenesis of charnockitic leucosomes of the Socorro-Guaxupé nappe. SE Brazil. Lithos 314–315, 16–39. https://doi.org/10.1016/j.lithos.2018.05.014.

Rocha, B.C., Campos Neto, M.C., Cioffi, C.R., Westin, A., Alves, A., Salazar-Mora, C.A., Egydio-Silva, M., Moraes, R., Souza, S.S., Maurer, V.C., 2024. The passive margin of the south São Francisco paleocontinent, metamorphic record and implications for the assembly of West Gondwana: evidence from the Lima Duarte Nappe, Ribeira Orogen (SE Brazil). Precambr. Res. Accept. Pap.

Rubatto, D., 2002. Zircon trace element geochemistry: partitioning with garnet and the link between U-Pb ages and metamorphism. Chem. Geol. 184, 123–138.

Rubatto, D., 2017. Zircon: the metamorphic mineral. Rev. Mineral. Geochem. 261–295. https://doi.org/10.2138/rmg.2017.83.09.

Santos, T.J.S., da Garcia, M.G.M., Amaral, W.S., Caby, R., Wernick, E., Arthaud, M.H., Dantas, E.L., Santosh, M., 2009. Relics of eclogite facies assemblages in the Ceará Central Domain, NW Borborema Province, NE Brazil: implications for the assembly of West Gondwana. Gondw. Res. 15, 454–470. https://doi.org/10.1016/j.gr.2009.01.003.

Santos, T.J.S., da Amaral, W.S., Ancelmi, M.F., Pitarello, M.Z., Fuck, R.A., Dantas, E.L., 2015. U-Pb age of the coesite-bearing eclogite from NW Borborema Province, NE Brazil: implications for western Gondwana assembly. Gondw. Res. 28, 1183–1196. https://doi.org/10.1016/j.gr.2014.09.013.

Santos, M.M., Lana, C., Scholz, R., Buick, I., Schmitz, M.D., Kamo, S.L., Gerdes, A., Corfu, F., Tapster, S., Lancaster, P., Storey, C.D., Basei, M.A.S., Tohver, E., Alkmim, A., Nalini, H., Krambrock, K., Fantini, C., Wiedenbeck, M., 2017. A new appraisal of Sri Lankan BB zircon as a reference material for LA-ICP-MS U-Pb geochronology and Lu-Hf isotope tracing. Geostand. Geoanal. Res. 41, 335–358. https://doi.org/10.1111/ggr.12167.

Santos, P.S., 2011. Geocronologia, área-fonte e ambiente tectônico da unidade Santo Antônio - Megassequência Andrelândia. Dissertação de Mestrado - Instituto de Geociências, Universidade Federal do Rio de Janeiro.

Schertl, H.P., Schreyer, W., Chopin, C., 1991. The pyrope-coesite rocks and their country rocks at Parigi, Dora Maira Massif, Western Alps: detailed petrography, mineral chemistry and PT-path. Contrib. Mineral. Petrol. 108, 1–21. https://doi.org/10.1007/BF00307322.

Schönig, J., von Eynatten, H., Tolosana-Delgado, R., Meinhold, G., 2021. Garnet major-element composition as an indicator of host-rock type: a machine learning approach using the random forest classifier. Contrib. Mineral. Petrol. 176, 1–21. https://doi.org/10.1007/s00410-021-01854-w.

Silva, M.P., 2010. Modelamento metamórfico de rochas das fácies xisto-verde e anfibolito com o uso de pseudoseções: exemplo das rochas da Klippe Carrancas, sul de Minas Gerais. Unpublished Master's Dissertation - Instituto de Geociências, Universidade de São Paulo.

Sláma, J., Košler, J., Condon, D.J., Crowley, J.L., Gerdes, A., Hanchar, J.M., Horstwood, M.S.A., Morris, G.A., Nasdala, L., Norberg, N., Schaltegger, U., Schoene, B., Tubrett, M.N., Whitehouse, M.J., 2008. Plešovice zircon — a new natural reference material for U-Pb and Hf isotopic microanalysis. Chem. Geol. 249, 1–35. https://doi.org/10.1016/j.chemgeo.2007.11.005.

Smith, D.C., 1984. Coesite in clinopyroxene in the Caledonides and its implications for geodynamics. Nature 310, 641–644. https://doi.org/10.1038/310641a0.

Sobolev, N.V., Shatsky, V.S., 1990. Diamond inclusions in garnets from metamorphic rocks: a new environment for diamond formation. Nature 343, 742–746. https://doi.org/10.1038/343742a0.

Stepanov, A.S., Rubatto, D., Hermann, J., Korsakov, A.V., 2016. Special collection: advances in ultrahigh-pressure metamorphism: contrasting P-T paths within the Barchi-Kol UHP terrain (Kokchetav Complex): implications for subduction and exhumation of continental crust. Am. Mineral. 101, 788–807. https://doi.org/10.2138/am-2016-5454.

Sun, S.-S., McDonough, W.F., 1989. Chemical and isotopic systematics of oceanic basalts: implications for mantle composition and processes. Geol. Soc. Lond. Spec. Publ. 42, 313–345.

Tedeschi, M., Pedrosa-Soares, A., Dussin, I., Lanari, P., Novo, T., Pinheiro, M.A.P., Lana, C., Peters, D., 2018. Protracted zircon geochronological record of UHT garnet-free granulites in the Southern Brasília orogen (SE Brazil): petrochronological constraints on magmatism and metamorphism. Precambr. Res. 316, 103–126. https://doi.org/10.1016/j.precamres.2018.07.023.

Toledo, B., Janasi, V.A., da Silva, L., 2018. SHRIMP U-Pb geochronology of the Socorro batholith and implications for the Neoproterozoic evolution in SE Brazil. Braz. J. Geol. 48, 761–782. https://doi.org/10.1590/2317-4889201820180040.

Tomkins, H.S., Powell, R., Ellis, D.J., 2007. The pressure dependence of the zirconium-in-rutile thermometer. J. Metam. Geol. 25, 703–713. https://doi.org/10.1111/j.1525-1314.2007.00724.x.

Triantafyllou, A., Berger, J., Baele, J.-M., Mattielli, N., Ducea, M.N., Sterckx, S., Samson, S., Hodel, F., Ennih, N., 2020. Episodic magmatism during the growth of a Neoproterozoic oceanic arc (Anti-Atlas, Morocco). Precambr. Res. 339, 105610 https://doi.org/10.1016/j.precamres.2020.105610.

Trouw, R.A.J., Ribeiro, A., Paciullo, F.V.P., 1980. Evolução estrutural e metamórfica de uma área a SE de Lavras - Minas Gerais. In: XXXI Congresso Brasileiro de Geologia - Anais.. SBG, Balneário de Camboriú, pp. 2773–2784.

Trouw, R.A.J., Paciullo, F.V.P., Ribeiro, A., 1998. Tectonic significance of Neoproterozoic high pressure granulites in southern Minas Gerais. In: 14 International Conference on Basement Tectonics. Ouro Preto, pp. 69–71.

Trouw, R.A.J., Heilbron, M., Ribeiro, A., Paciullo, F.V.P., Valeriano, C.M., Almeida, J.C.H., Tupinambá, M., Andreis, R.R., 2000. The central segment of the Ribeira Belt. In: Cordani, U.G., Milani, E.J., Thomaz Filho, A., Campos, D.A. (Eds.), Tectonic Evolution of South America. 31 International Geological Congress, Rio de Janeiro, pp. 335–365.

Trouw, R.A.J., Paciullo, F.V.P., Ribeiro, A., Bittar, S., Almeida, J.C.H., 2002. Mapa Geológico - Folha Caxambú.

Trouw, R.A.J., Ribeiro, A., Paciullo, F.V.P., 1983. Geologia estrutural dos grupos São João del Rei, Carrancas e Andrelândia, sul de Minas Gerais. An. Acad. Bras. Cienc. 55, 71–85.

Trouw, R.A.J., Ribeiro, A., Paciullo, F.V.P., 1986. Contribuição à geologia da Folha Barbacena. In: XXXIV Congresso Brasileiro De Geologia. SBG, Goiânia, pp. 974–984.

Trouw, C.C., 2008. Mapeamento da Folha Virgínia - MG, geocronologia U-Pb (SHRIMP) em zircões e interpretação geotectônica. Instituto de Geociências - Universidade Federal do Rio de Janeiro.

Valeriano, C.M., 2017. The Southern Brasília Belt. In: Heilbron, M., Cordani, U., Alkmim, F. (Eds.), São Francisco Craton, Eastern Brazil. Regional Geology Reviews. Springer, Cham.

Vannay, J.-C., Grasemann, B., 2001. Himalayan inverted metamorphism and syn-convergence extension as a consequence of a general shear extrusion. Geol. Mag. 138, 253–276.

Vavra, G., Schmid, R., Gebauer, D., 1999. Internal morphology, habit and U-Th-Pb microanalysis of amphibolite-to-granulite facies zircons: geochronology of the Ivrea Zone (Southern Alps). Contrib. Mineral. Petrol. 134, 380–404. https://doi.org/10.1007/s004100050492.

Vinagre, R., Trouw, R.A.J., Mendes, J.C., Duffles, P., Peternel, R., Matos, G., 2014. New evidence of a magmatic arc in the southern Brasília Belt, Brazil: the Serra da Água Limpa batholith (Socorro-Guaxupé Nappe). J. S. Am. Earth Sci. 54, 120–139.

Walters, J.B., 2022. MinPlot: a mineral formula recalculation and plotting program for electron probe microanalysis. Mineralogia 53, 52–67. https://doi.org/10.2478/mipo-2022-0005.

Wang, A., Freeman, J.J., Jolliff, B.L., 2015. Understanding the Raman spectral features of phyllosilicates. J. Raman Spectrosc. 46, 829–845. https://doi.org/10.1002/jrs.4680.

Warr, L.N., 2021. IMA–CNMNC approved mineral symbols. Mineral. Mag. 85, 291–320. https://doi.org/10.1180/mgm.2021.43.

Watson, E.B., Wark, D.A., Thomas, J.B., 2006. Crystallization thermometers for zircon and rutile. Contrib. Mineral. Petrol. 151, 413–433.

Webb, A.A.G., Yin, A., Harrison, T.M., Célérier, J., Burgess, W.P., 2007. The leading edge of the Greater Himalayan Crystalline complex revealed in the NW Indian Himalaya: implications for the evolution of the Himalayan orogen. Geology 35, 955–958. https://doi.org/10.1130/G23931A.1.

Westin, A., Campos Neto, M.C., 2013. Provenance and tectonic setting of the external nappe of the Southern Brasília Orogen. J. S. Am. Earth Sci. 48, 220–239.

Westin, A., Campos Neto, M.C., Hawkesworth, C.J., Cawood, P.A., Dhuime, B., Delavault, H., 2016. A Paleoproterozoic intra-arc basin associated with a juvenile source in the Southern Brasilia Orogen: application of U-Pb and Hf-Nd isotopic analyses to provenance studies of complex areas. Precambr. Res. 276, 178–193. https://doi.org/10.1016/j.precamres.2016.02.004.

Westin, A., Campos Neto, M.C., Cawood, P.A., Hawkesworth, C.J., Dhuime, B., Delavault, H., 2019. The Neoproterozoic southern passive margin of the São Francisco craton: insights on the pre-amalgamation of West Gondwana from U-Pb and Hf-Nd isotopes. Precambr. Res. 320, 454–471. https://doi.org/10.1016/j.precamres.2018.11.018.

Westin, A., Campos Neto, M.C., Hollanda, M.H.B.M., Salazar-Mora, C.A., Queiroga, G., Frugis, G.L., de Castro, M.P., 2021. The fast exhumation pattern of a Neoproterozoic nappe system built during West Gondwana amalgamation: insights from thermochronology. Precambr. Res. 355, 106115.

Whitney, D.L., Cooke, M.L., Du Frane, S.A., 2000. Modeling of radial microcracks at corners of inclusions in garnet using fracture mechanics. J. Geophys. Res. Solid Earth 105, 2843–2853. https://doi.org/10.1029/1999JB900375.

Wu, Y., Fei, Y., Jin, Z., Liu, X., 2009. The fate of subducted Upper Continental Crust: an experimental study. Earth Planet. Sci. Lett. 282, 275–284. https://doi.org/10.1016/j.epsl.2009.03.028.

Ye, K., Cong, B., Ye, D., 2000. The possible subduction of continental material to depths greater than 200 km. Nature 407, 734–736. https://doi.org/10.1038/35037566.

Zhang, L., Ellis, D., Williams, S., Jiang, W., 2003. Ultrahigh-pressure metamorphism in eclogites from the western Tianshan, China - Reply. Am. Mineral. 88, 1157–1160.

Zhang, M., Liu, W., Guan, L., Takahata, N., Sano, Y., Li, Y., Zhou, X., Chen, Z., Cao, C., Zhang, L., Lang, Y.-C., Liu, C.-Q., Xu, S., 2022. First estimates of hydrothermal helium fluxes in continental collision settings: insights from the southeast Tibetan Plateau margin. Geophys. Res. Lett. 49, e2022GL098228 https://doi.org/10.1029/2022GL098228.

Zhang, L., Wang, Y., 2020. The exhumation of high- and ultrahigh-pressure metamorphic terranes in subduction zone: questions and discussions. Sci. China Earth Sci. 63, 1884–1903. https://doi.org/10.1007/s11430-020-9579-3.

Zhang, M., Xu, S., Zhou, X., Caracausi, A., Sano, Y., Guo, Z., Zheng, G., Lang, Y.-C., Liu, C.-Q., 2021. Deciphering a mantle degassing transect related with India-Asia continental convergence from the perspective of volatile origin and outgassing. Geochim. Cosmochim. Acta 310, 61–78. https://doi.org/10.1016/j.gca.2021.07.010.

Zheng, Y.-F., 2009. Fluid regime in continental subduction zones: petrological insights from ultrahigh-pressure metamorphic rocks. J. Geol. Soc. Lond. 166, 763–782. https://doi.org/10.1144/0016-76492008-016R.

Zheng, Y.-F., 2012. Metamorphic chemical geodynamics in continental subduction zones. Chem. Geol. 328, 5–48. https://doi.org/10.1016/j.chemgeo.2012.02.005.

Zheng, Y.-F., Zi-Fu, Z., Ren-Xu, C., 2019. Ultrahigh-pressure metamorphic rocks in the Dabie-Sulu orogenic belt: compositional inheritance and metamorphic modification. Geol. Soc. Lond. Spec. Publ. 474, 89–132. https://doi.org/10.1144/SP474.9.